DIPLOMA THESIS

Investigation on the Effect of Reynolds Number on Pneumatic Three-Hole Pressure Probe Calibration

by

Rafel Giralt i Cubi

under direction of

Dr.techn. R.Willinger

A thesis submitted to the

Institute for Thermodynamics and Energy Conversion

of the Vienna University of Technology

in partial fulfilment of the

requirements for the degree of

Industrial Engineer

Department of Turbomachines

February 2008

Abstract

The aim of the present diploma thesis is the investigation the effect of the Reynolds number on the calibration of different three-hole pressure probes. The work has been carried out in the free jet wind tunnel of the Vienna University of Technology.

We can also find a descripction of the main characteristics of the three-hole probe geometries available in the institute that have been used in this work.
The experiment has been performed with the probes in nulling position, following the secuence that consist in increase and afterwards decrease the velocity of the airflow, in order to find, if it exists, a case of hysteresis in fluid dynamics.

We have obtained that all the calibration coefficients except k_1, k_t and k_β show variation respect Reynolds number. However, in view of the results, we cannot affirm that hysteresis has appeared with enough clearness, because it also could be interpreted as a slight deviation or fluctuation of the measures.

Acknowledgements

Let me begin dedicating the first lines of the following work at European Union which through Lifelong Learning Programme - Higher Education (ERASMUS), has given me the opportunity to finalize my degree in Austria. Together with an enriched study experience, Erasmus also provides exposure to different cultures and people around all Europe.

I would like to give my most sincere thanks at Dr. techn. Reinhard Willinger, I am glad to have worked under his direction. Without his support this work could have never been possible.

And finally, I would like to thank at the Institute of Thermodynamics and Energy Conversion of the Vienna University of Technology for allow me develop this present work at their facilities.

Contents

List of Tables

List of Figures

Nomenclature

a	[m]	Side hole spacing
d	[m]	Probe width
d_n	[m]	Nozzle exit diameter
f	[-]	Frequency of vortex shedding
k_i	[-]	Hole coefficient
$\bar{k}$	[-]	Mean hole coefficient
k_β	[-]	Direction coefficient
k_d	[-]	Dynamic pressure coefficient
k_s	[-]	Static pressure coefficient
k_t	[-]	Total pressure coefficient
Ma	[-]	Mach number
n	[rpm]	Rotational speed
$\bar{p}$	[Pa]	Mean hole pressure
p_i	[Pa]	Pressure sensed by the hole i
p_t	[Pa]	Total pressure
p_a	[Pa]	Ambient pressure
Re	[-]	Reynolds number
St	[-]	Strouhal number
T	[°C]	Temperature
T_a	[°C]	Ambient temperature
w	[m/s]	Velocity
w_0	[m/s]	Speed of sound in undisturbed medium

L	[m]	Characteristic length
C_D	[-]	Drag coefficient
C_L	[-]	Lift coefficient
α	[°]	Angle of attack
β	[°]	Yaw angle
δ	[°]	Wedge angle
φ	[°]	Angular coordinate
μ	$[Kg/(m \cdot s)]$	Dynamic viscosity
ν	$[m^2/s]$	Kinematic viscosity
ρ	$[Kg/m^3]$	Density

Subscripts

d	related to probe diameter
i	1,2,3 related to hole number

Abbreviation

CDF	Computational fluid dynamics
DC	Direct current

Chapter 1

Introduction and Motivation

This work part of a previous thesis carried out by Mr. D.Lerena [3], under direction of Dr.techn. R.Willinger in the same institute of Thermodynamics and Energy Conversion of Vienna University of Technology. They calibrated some three-hole probes with different head geometries at a constant pitch angle and Reynolds number. The aim of that work was to obtain the calibration curves of some coefficients versus a defined range of yaw angle positions.

The idea of try to find a relation between hysteresis in a fluid flow and the calibration of the probes appears through the calibration data supplied by the manufacturer of one of the probes employed in this work, SVUSS/3 cobra head probe.

This data showed a transition zone of a non-dimensional parameter that express the relation between total and static pressure over the Reynolds number, which can be interpreted as a behavior of the dynamic pressure. The measurements supplied by the manufacturer contains sequences where the Reynolds number is arise and decrease progressively. Fig.1.1 shows this particularity.

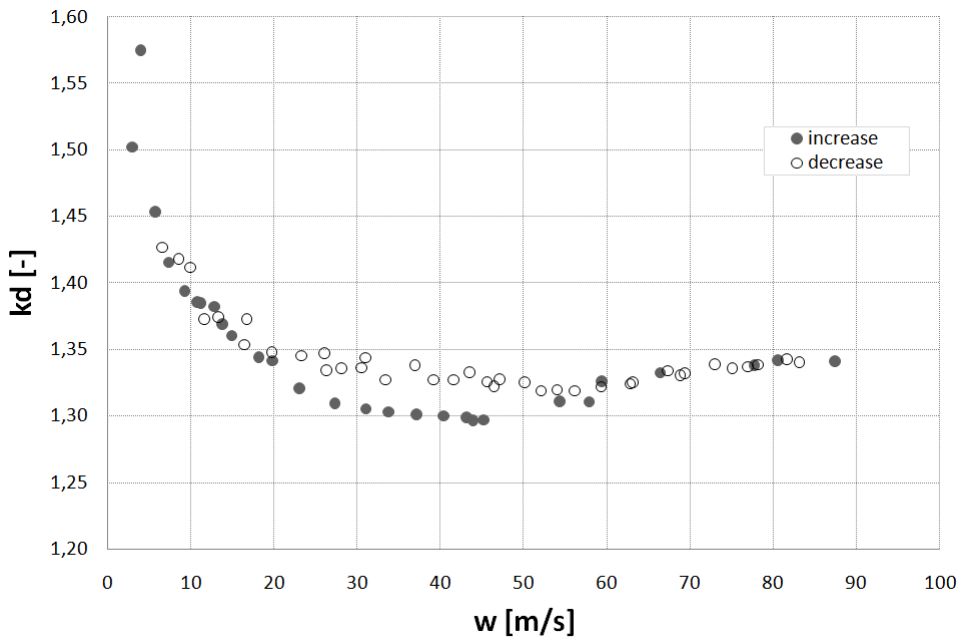

Figure 1.1: SVUSS/3 data provided by manufacturer

The transition zone was not clearly defined, but the data has been selected to make it clear. It could be interpreted as an inherent scatter of data acquisition and experimental procedure. The fact that the hysteresis in fluidynamic is not a usual case was the main motivation to make this work. The data provided by the manufacturer it will be checked with our own data, which will be obtained experimentally at facilities of the institute mentioned above. Finally we will discuss the results and we will look for possible explanations for this phenomenon.

Chapter 2

Literature Survey

2.1 Reynolds Number Effects on Calibration of Multi-hole Pressure Probes

There are many articles related with this topic that have been published in some specialized magazines and journals, what provide us a valuable background of documentation to consult. In these papers basically is performed the experimental calibration of some probes. Studying which are the factors that have influence on the calibration of the probe. Because calibration is a necessary step to do before to start to use the probe in a concrete turbomachinery application, such as flow measurement in a rotor blade passage, the wake occurred in the propeller plane of a surface ship model, and so on.

Treaster and Yocum [8] calibrated a five-hole prism probe at different yaw and pitch angles range. To investigate its effects, the probes were calibrated in the open-

jet facility over a Reynolds number range from $2 \cdot 10^3$ up to $7 \cdot 10^3$. From their analysis they concluded that the total pressure, pitch and yaw coefficients were essentially unaffected by the Reynolds number variation. Nevertheless, a measurable change in the static pressure coefficient was observed. Also investigated was the effect of wall vicinity on the calibration data obtained for the prism probe. Calibrations were conducted for a probe approaching normal to a flat plate aligned parallel to the reference flow. Only the static pressure coefficient exhibited significant changes. For the probe being withdrawn through the plate, all calibration coefficients were altered within two probe diameters of the wall; however, at distance greater than two probe diameters from the wall, only the static pressure coefficient was influenced.

Sitaram et al. [7] performed an experiment within the blade passages of an axial flow compressor and an axial flow inducer employing a five-hole probe, a disk probe and a spherical head static-stagnation pressure probe. They estimate how to estimate and evaluate the source of the errors and how these affect in particular at each probe. Turbulence, Reynolds and Mach number, rotation, pressure and velocity gradients, wall vicinity, probe blockage and probe stem; all these effects were studied and documented how to estimate their magnitude.

Dominy and Hodson [1] studied effects of the Reynolds number, Mach number and turbulence on the calibrations of commonly used cone-type and pyramid-head five-hole probes for a Reynolds numbers in range between $7 \cdot 10^3$ and $8 \cdot 10^4$. However, only the yaw angle was changed from -20 degrees to 20 degrees at a fixed zero pitch angle. They found very interesting results. They found the existence of two distinct

Reynolds number effects. One of them produces flow separation around the probe head at relatively low Reynolds numbers when the probe is at incidence. The other is related to changes in the detailed structure of the flow around the sensing holes even when the probe is nulled.

Lee and Jun [2] investigated the effects of the Reynolds number on the non-nulling calibration of a typical cone-type five-hole of 4,75mm in head diameter in the full range of the pitch and yaw angles for the Reynolds number more commonly encountered in turbomachinery applications. Concretely the calibrations were performed at six Reynolds numbers between $6.6 \cdot 10^3$ and $3.17 \cdot 10^4$, changing at each Reynolds number the pitch and yaw angles from -35 degrees to 35 degrees. They found that the effects on the pitch- and yaw-angle coefficients are significant when the absolute values of both are smaller than 20 degrees. The static-pressure coefficient is sensitive to the Reynolds number during all over pitch- and yaw-angle range. Nevertheless the total-pressure coefficient is appreciable when the absolute values of the pitch- and yaw-angles are larger than 20 degrees.

More closely related on the calibration of three-hole probes, Willinger [10], and Willinger and Haselbacher [9] analyzed how the streamline projection method can be used for an approximation of the influence of a velocity gradient as well to find out the influence of a wall proximity effect. At the first case, the velocity gradient induces a pressure difference between the lateral holes which is interpreted by the probe as a flow angle error which can be expressed as a linear relationship over the nondimensional velocity gradient. At the second case, the study of wall proximity

effects concluded that the hole near the wall sees a higher velocity than the freestream velocity. Thus if it is compared with the other lateral hole, the pressure difference is interpreted by the hole as a flow angle error which can be expressed as a nonlinear relationship over the nondimensional distance y/d from the wall to the probe. For both situations, the data obtained was checked with the results of a numerical investigation with CFD simulation. A good agreement is observed in direction coefficient as well as for the total pressure coefficient, however a roughly agreement are presented in hole coefficients. And finally great discrepancies between measurements, streamline projection method and simulated results for the static pressure coefficient.

2.2 Hysteresis Effects in Fluid Dynamics

Hysteresis is defined as system that may be in any number of states, independent of the inputs to the system. So this system exhibits path-dependence, or "rate-independent memory". In a system with hysteresis we can't predict the output without looking at the history of the input. This phenomenon is not commonly encountered in fluid dynamics, but it has been observed in several situations. The fact that is an extraordinary event makes that, in some cases, the reasons for why hysteresis appears are not well known.

2.2.1 Stall in the Diffusers [5]

The application of a diffuser is to decelerate the fluid passing the flow through it. The purpose is to convert as large a fraction as possible of the dynamic pressure into static pressure. To have steady and symmetric flow downstream of the diffuser is

at least equally important as the deceleration of the flow. The exit flow conditions and performance level of a diffuser are strongly related to the presence or absence of flow separation, also called stall, in the diffuser. The regions of stalled flow block off the flow, cause low pressure recovery, and usually result in severe flow asymmetry, unsteadiness, or both. Two important facts have to take in consideration, flow

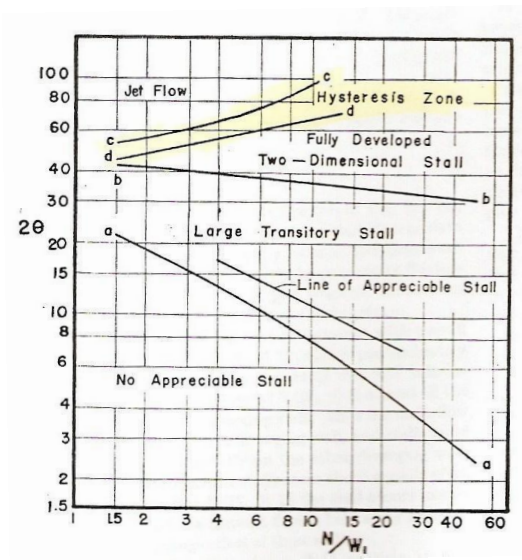

Figure 2.1: Flow regimes in striaght-wall, two dimensional diffusers.

conditions in and performance of unstalled and slightly stalled diffusers, are weakly affected by variations in Mach number and Reynolds number when Mach number is subsonic and inlet Reynolds number is greater than $5 \cdot 10^4$.

The spectrum of stall states for internal flow in a diffuser can be divided into four major patterns or flow regimes:

- No Appreciable Stall Regime: The pressure and velocity profiles are essentially

symmetrical about the center plane and are relatively constant in time.

- Large Transitory Stall Regime: The flow is very erratic. Stall regions are in constant forming in, and then washing out of the diffuser.

- Two-Dimensional Stall Regime: As its name indicates, a steady two-dimensional stall exists. The flow separates near the throat and follows one diverging wall. The stall remains on either wall, and blocks a significant fraction of the available flow area, but allows that the through-flow covers the other diverging wall.

- Jet Flow Regime: The incoming flow separates from both diverging walls very near the throat and proceeds straight down the diffuser; a large fixed stall covers each diverging wall. But in the jet flow regime, the velocity and pressure profiles are relatively steady except for the shear layer at the edges of the jet.

The reasons why hysteresis appeared were not discussed, only was commented its existence and the effect on the pressure recovery. But it seems to be related with the transition between flow regimes, due to it was observed that the time necessary for stall build-up is usually considerably larger than the necessary for stall washout.

2.2.2 Flow across Bluff-Bodies and Vortex Shedding [6]

A vortex is a spiral flow motion with closed streamline. This is spinning and often turbulent. The motion of the fluid swirling rapidly around a center is called a vortex. In free vortex, the speed and rate of rotation of the fluid are greatest at the center, and decrease progressively with distance from the center.

Vortex shedding is an unsteady flow that takes place in special flow velocities (according to the size and shape of the cylindrical body). In this flow, vortices are created at the back of the body and detach periodically from either side of the body. Vortex shedding is caused when air flows past a blunt object. The airflow past the object creates alternating low-pressure vortices on the downwind side of the object. The object will tend to move toward the low-pressure zone.

Over a large Reynolds number range, eddies are shed continuously from each side of the body, forming rows of vortices in its wake. The alternation leads to the core of a vortex in one row being opposite the point midway between two vortex cores in the other row. Ultimately, the energy of the vortices is consumed by viscosity as they move further down stream and the regular pattern disappears.

When a vortex is shed, an unsymmetrical flow pattern forms around the body, which therefore changes the pressure distribution. This means that the alternate shedding of vortices can create periodic lateral forces on the body in question, causing it to vibrate. If the vortex shedding frequency is similar to the natural frequency of a body or structure, it causes resonance.

Strouhal number is a dimensionless number that describes these oscillating flow mechanisms.

$$St = \frac{fL}{w} \tag{2.1}$$

where f is the frequency of vortex shedding, L is the characteristic length and w is the velocity of the fluid.

The Reynolds number plays an important role here because flow separations are often Reynolds number dependent, even if the bodies have sharp edges. The reason for this dependence is that the state of the boundary layer has a far-reaching influence on the entire flow field about a body. When the Reynolds number increases the flow separates of the body and bubble is formed, it becomes larger, then unstable and finally then bursts.

Airflow across smooth cylinder

The circular cylinder is the classical bluff body that exhibits strong Reynolds number effects. Schewe [6] studied the Reynolds number effects on flow around bluff-bodies, at following are commented the part of the work related with airflow across cylinder because hysteresis was observed in some coefficients.

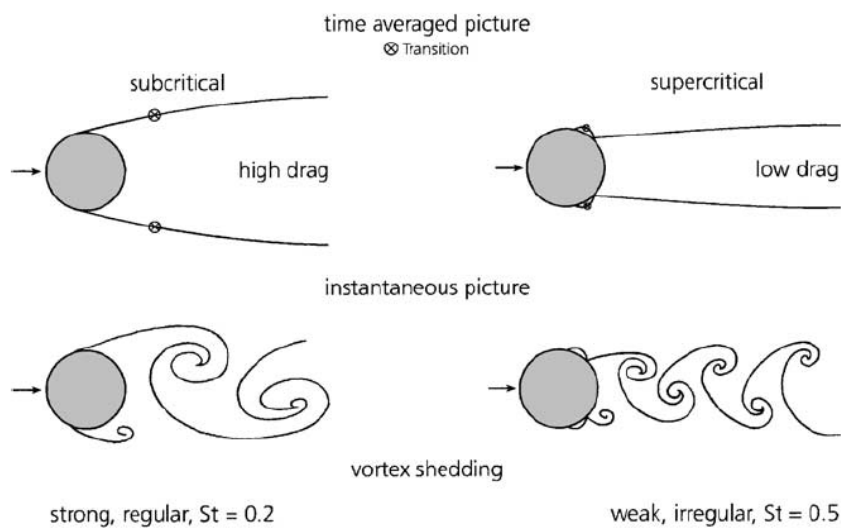

Figure 2.2: Example for strong Reynolds number effects.

Fig.2.2 illustrates the key role of the laminar/turbulent transition in flow past

a circular cylinder, both below and above the critical flow regime. The Reynolds number effects here are clearly evident and dramatic. These phenomena, which are triggered by the transition from laminar to turbulent flow, have characteristics that are universally valid because they occur in similar form in flow over bodies having other cross-sections.

To simplify somewhat, we can imagine that the separated shear layer undergoes transition (which occurs in the wake at low Reynolds numbers) at a point that wanders upstream as Reynolds number increases. If, at critical Reynolds numbers, the transition point reaches the surface of the body, separation bubbles could be formed. This process is accompanied by a decrease in the width of the wake (drag crisis) and, because of the unsteady behaviour, a jump in the value of the Strouhal number St.

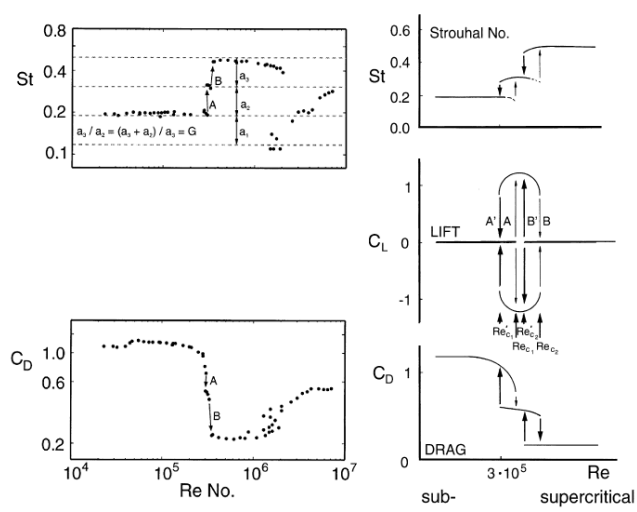

Figure 2.3: Strouhal, lift and drag coefficients for a smooth cylinder

Fig.2.3 shows a schematic representation of how the two transitions A and B in

the critical flow region are mirrored by the characteristic coefficients C_D; C_L; and *St*. With reference to the lift, the two transitions can be interpreted as subcritical bifurcations at two critical Reynolds numbers. Both transitions are distinguished by a discontinuous decline of drag, a jump in the value of the Strouhal number, and hysteresis effects.

Von Karman Vortex Street

A vortex street will only be observed over a given range of Reynolds numbers, typically above a limiting Reynolds number value of about 90. The range of Reynolds number values will vary with the size and shape of the body from which the eddies are being shed, as well as with the kinematic viscosity of the fluid.

A particular vortex street situation was studied by Von Karman. It is a repeating pattern of swirling vortices caused by the unsteady separation of flow over bluff bodies. This case illustrates Strouhal instability and the particular wake known as Von Karman Vortex Street. It is a succession of vortices created close to the cylinder that break away alternatively from both sides of the cylinder. Vortices are emitted regularly and rotate in opposite senses.

Figure 2.4: Example of Von Karman vortex street.

2.2.3 Static Stall of an Airfoil [4]

This phenomenon is not very well understood. It happens in particular positions of an airfoil when a airflow goes around on it. It is caused by massive flow separation resulting in sharp drop in lift and increase in the drag acting on the airfoil. The prediction of the hysteresis associated at this phenomenon was studied by S. Mittal and P. Saxena. They made an effort to study the behavior of the flow near stall, over the body NACA 0012 airfoil, by solving the governing equations numerically. The analytical results were compared with experimental ones as we can see at Fig.2.5.

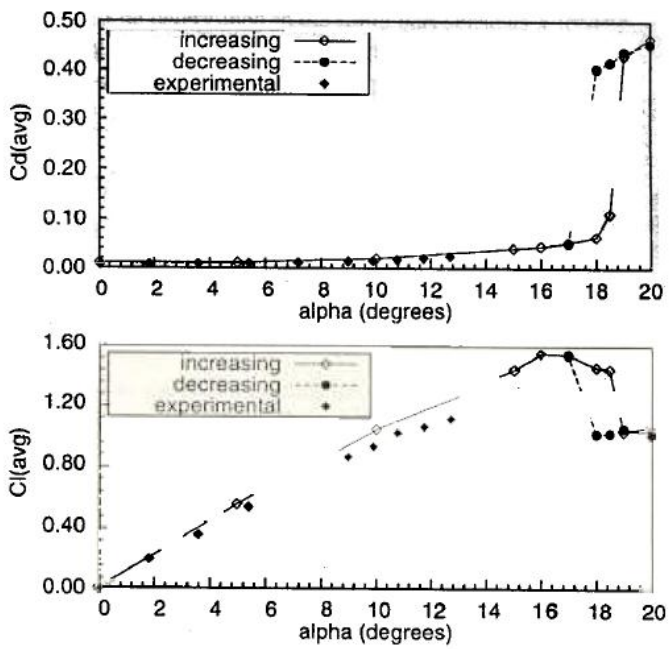

Figure 2.5: Variation of the time-averaged drag and lift coefficients

The experiment results correspond to $Ma = 0.3$ and $Re = 1.8 \cdot 10^6$ flow. From 0 to 16 degrees ot attack angle the trend of the time-averaged drag and lift coefficients is almost linear. Suddenly it can be observed that hysteresis appears for angles of

attack close to the stall angle. The computations indicated that the flow ceases to be steady beyond $\alpha = 17$ deg and vortex shedding was observed at Fig.2.6.

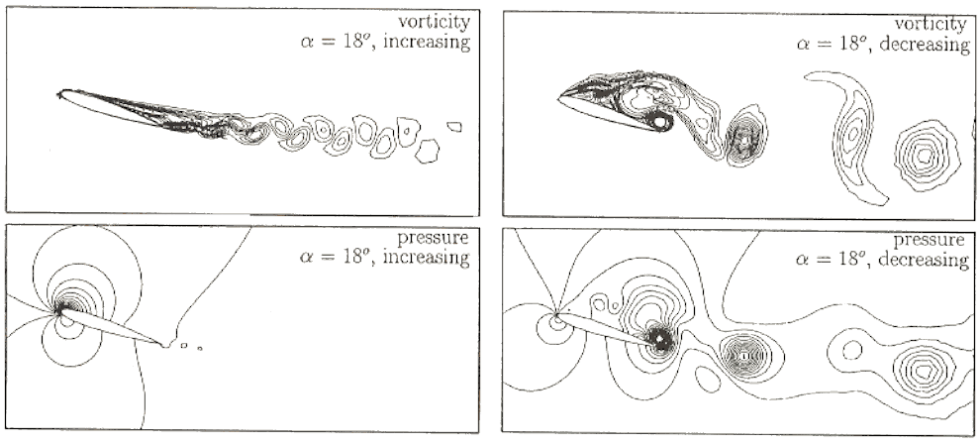

Figure 2.6: Vorticity and pressure fields for the computed solutions

Their arguments about how to explain the hysteresis behavior appeared were that the flow has the ability to remember its past history. For the same angle of attack, the flow obtained with the increasing angle results in an almost attached flow with higher lift and lower drag, whereas the one with decreasing angle of attack is associated with large unsteadiness, lower lift, and higher drag.

Chapter 3

Geometry of the Probes

Multi-hole probes are commercially available in several configurations. These can be classified in two main groups: by geometry shape or by the number of sensing holes. However, the combination of both permits find probes of a concrete geometry with 3, 5 or 7 holes.

The most common shapes for probes head geometries are: cobra head, trapezoidal head and cylindrical. Prismatic and cone forms are used as well, but due to their less streamlined shape the calibration has to be done completely empirical. The most well known and widely used are the three-hole pressure probes, as the name indicate are characterized by three pressure sensing holes lying in one plane, which ones are used in the present work.

These have mainly three different types of head geometries: cobra, trapezoidal and cylinder head. The head shape and hole arrangements are plotted in Fig.3.1 where the yaw angle is also identified.

The probes when are introduced in a flow field create a flow disturbance due to is

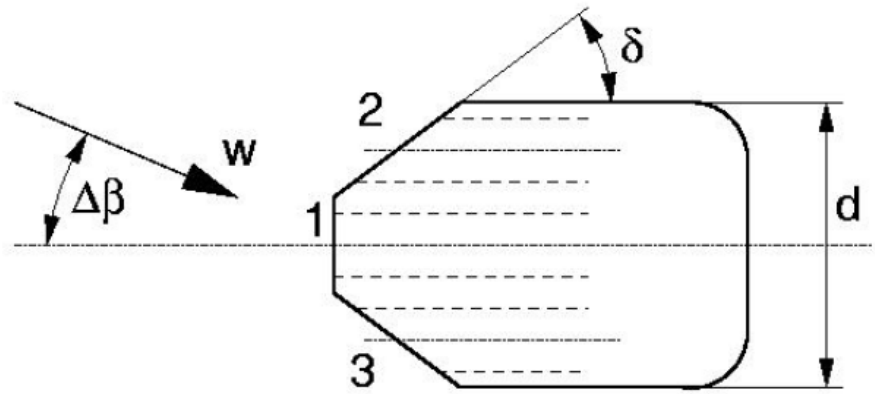

Figure 3.1: Three-hole Probes geometry

an intrusive method to measure. Thus, in order to minimize its disturbance effects in the flow field the geometry of the probes are characterized for a slender body, where the width must be much less than the length. So the probes are a measurement instrument generally miniaturized.

A summary of the main characteristics of the probes employed in this work are defined in Table 3.1.

Probe Geometry	d[mm]	δ[°]	a[mm]	Thermocouple
SVUSS/3 Cobra Probe	2.4	30	1.6	No
AVA 110 Trapezoidal Probe	3.3	30	2.0	Yes
AVA 43 Cylinder Probe	3.0	50	2.3	No

Table 3.1: Three-hole Probes characteristics

3.1 SVUSS/3 Cobra Probe

A picture of the cobra probe is shown in Fig.3.2. It shows clearly the cobra shape of the head which gives the name to the probe. The probe was manufactured by the SVUSS company in Czech Republic at 1994. Its characteristic dimensions are the following: the probe head is 2.4mm in width and 0.8mm in height, and the total length is 650mm. The three holes are 0.5mm in diameter, drilled and disposed in the same plane, parallel to the axis of the probe. Thus the sensing area is facing forward into the flow. The distance between the two lateral holes is 1.6mm.

Figure 3.2: SVUSS/3 Cobra Probe

Although is named as cobra head probe, its head geometry is trapezoidal with a characteristic wedge angle $\delta = 30°$. The characteristic dimensions are shown in Fig.3.5. Each hole conducts the pressure sensed through three independent tubes to the pressure transducer. The central hole measures approximately the stagnation pressure and the outer holes determine a pressure difference which is interpreted by the probe, after to be calibrated, as a yaw angle direction of the flow.

3.2 AVA 110 Trapezoidal Probe

The AVA probe number 110 was manufactured at 1968 by Aerodynamische Versuchsanstalt Göttingen E.V.

The characteristics dimensions of this probe are defined with a total length equal to 366mm and the body is 6mm in diameter. Like the cobra probe, the sensing area is forward facing and the head geometry is trapezoidal with a wedge angle $\delta = 30°$. The diameter of the holes is 0.6mm and the side ones are separated 2.0mm. The characteristic dimensions of the probe head are 3.3mm in width and 1.3mm in height.

The three tubes which conducts the pressure are bundled together as it can be observed in Fig.3.4. The probe includes a thermocouple sensor to measure the flow's temperature.

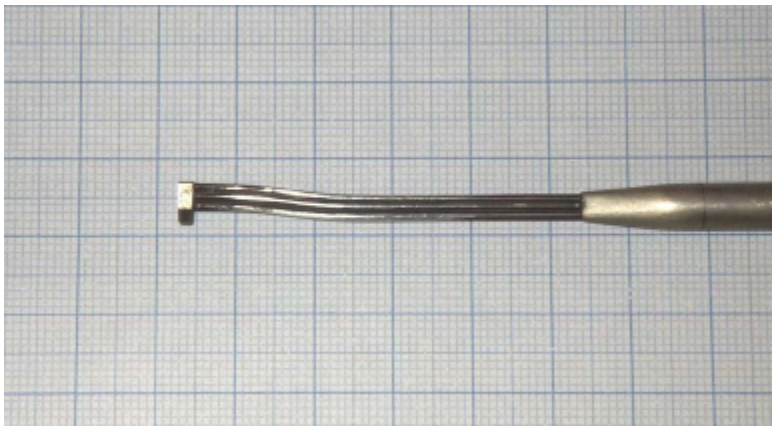

Figure 3.3: AVA trapezoidal probe Nr.110

The characteristic dimensions are shown with more precision in Fig.3.6.

3.3 AVA 43 Cylinder Probe

AVA cylinder probe number 43 was manufactured by Aerodynamische Versuchsanstalt Göttingen E.V.

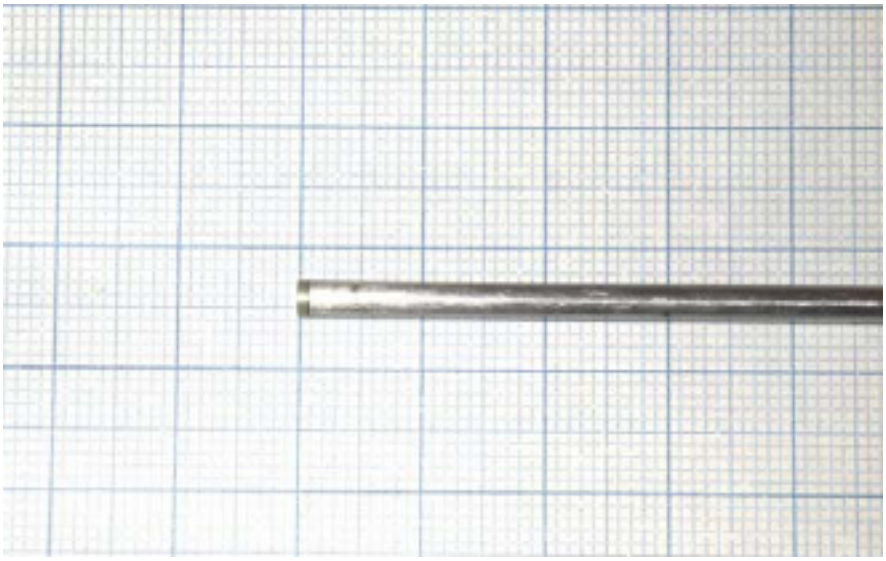

Figure 3.4: AVA 43 Cylinder Probe

As its name indicates, the head geometry of this probe is a cylinder of 3.00mm in diameter, which is the characteristic dimension. The characteristic angle is $\delta = 50°$ and defines the position of the outer holes respect the perpendicular plane of the probe axis.

The probe is shown in Fig.3.4. Its total length is 335mm and the diameter of the main body is 6mm. The central hole number 1 is 0.3mm in diameter and the outer holes are 0.6mm diameter, being the distance between these two holes of 2.3mm. The characteristic dimensions are shown with more precision in Fig.3.7.

Figure 3.5: Drawing of the SVUSS/3 cobra probe

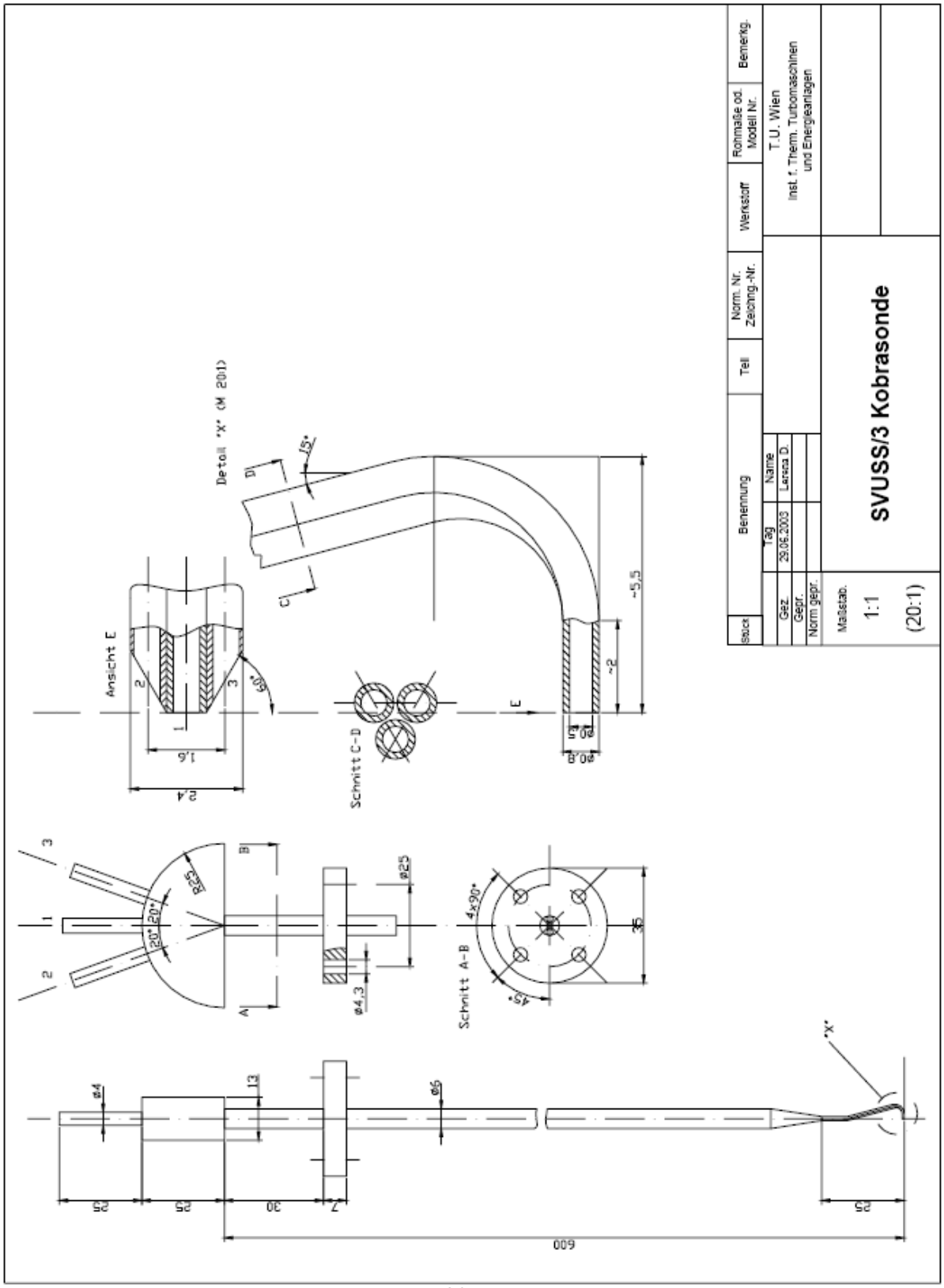

Figure 3.6: Drawing of the AVA 110 trapezoidal probe

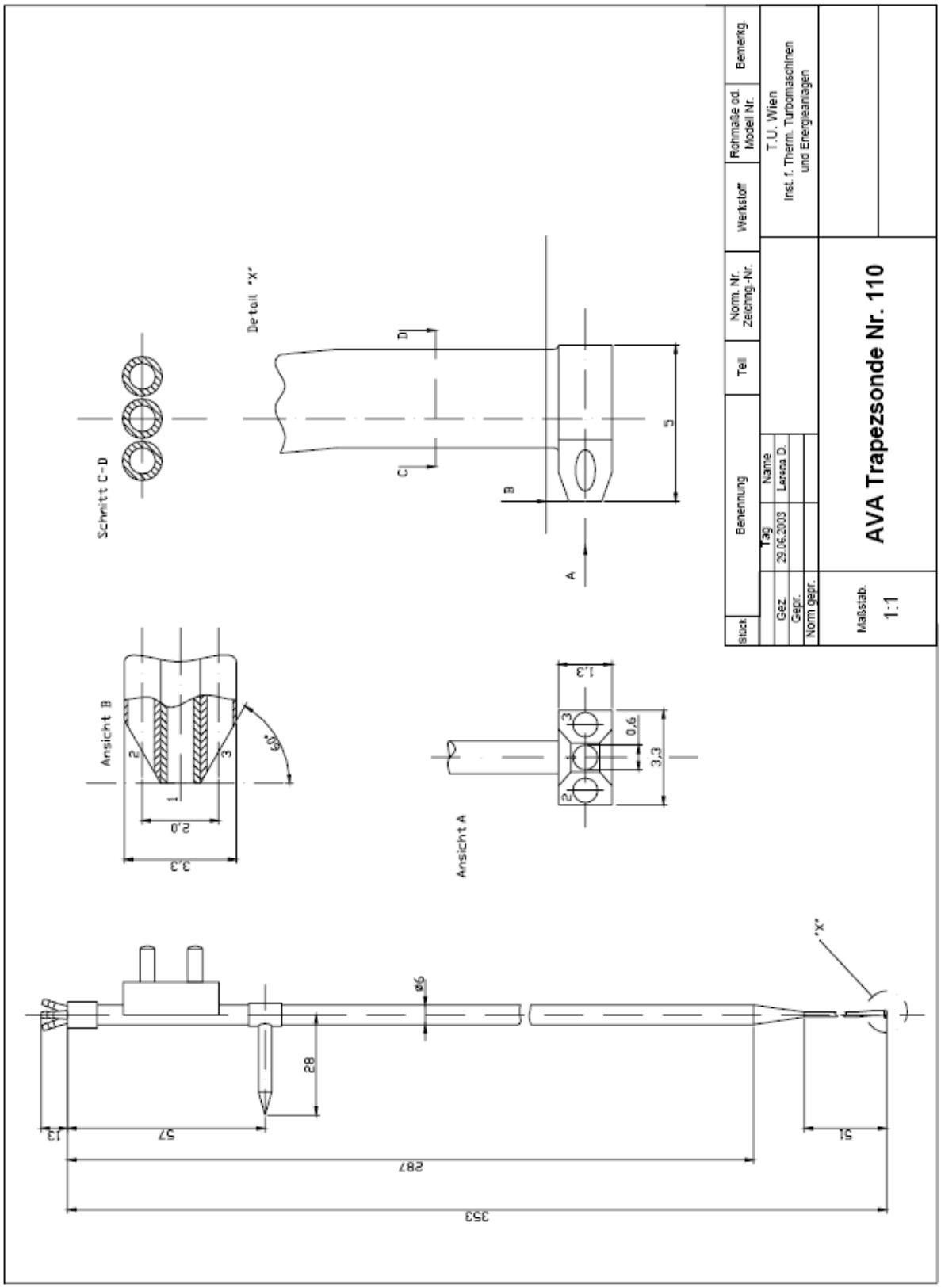

Figure 3.7: Drawing of the AVA 43 cylinder probe

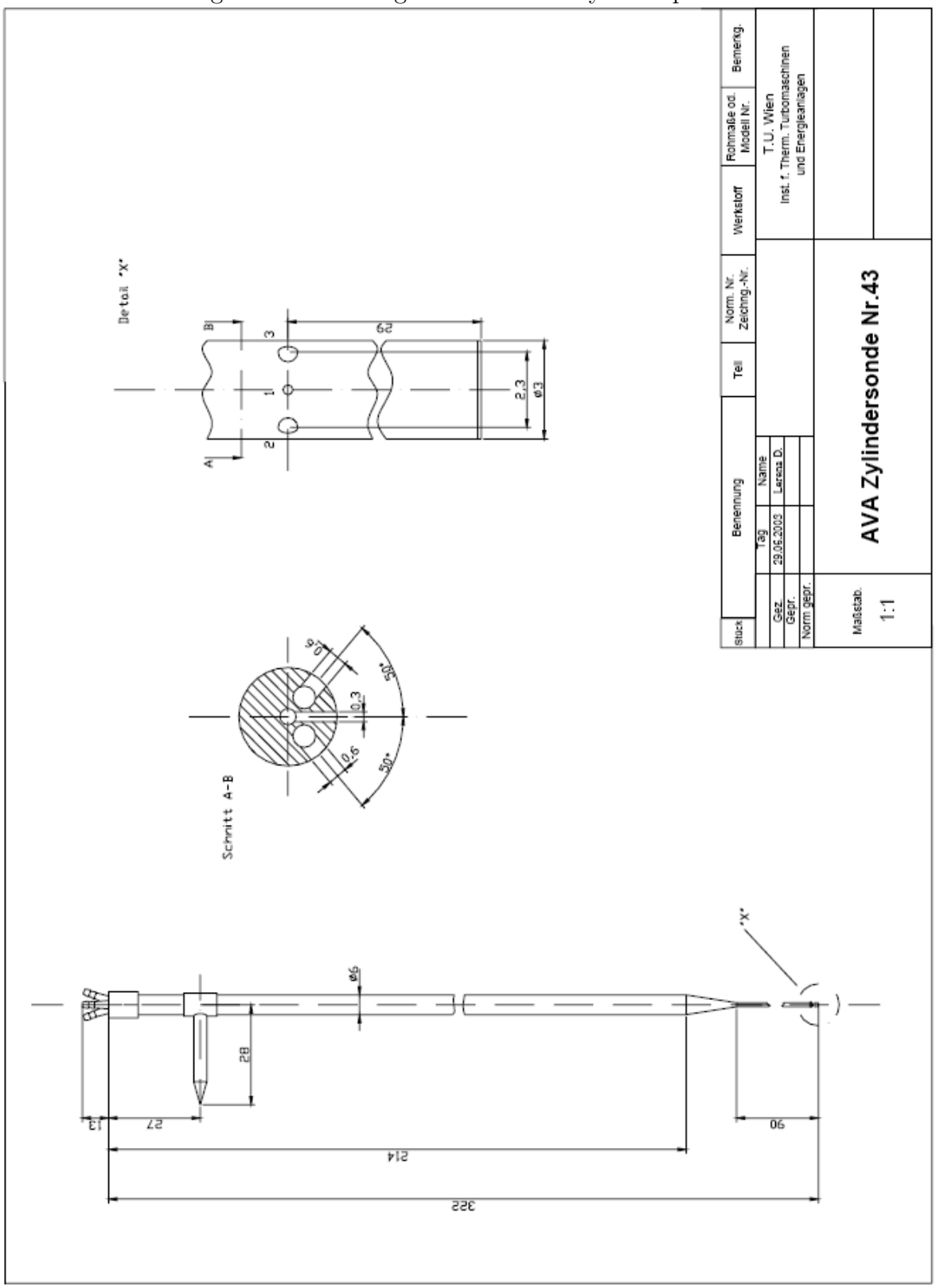

Chapter 4

Experimental Calibration

4.1 About the Calibration

In many complex flow fields such as those encountered in turbomachines, the experimental determination of the steady-state three-dimensional characteristics of the flow field are frequently required. This application requires calibration data which are not usually supplied by the manufacturer. Thus, the measurement of these data and the development of an interpolation procedure become the responsibility of the user.

Due to nature of this work it is important to define the most important characteristics of the measurement systems. Even though we can distinguish between two main groups: static and dynamic characteristics, it is only considered the first one because is more relevant for this experimental analysis. The static characteristics of an instrument describe the behavior of variables that change very slowly. In these cases, the instrument has time enough to reach the steady point before take the next

measure. The set: probe and piezoresisitve transducer, is the instrument of measure used in this work. The following are the most important parameters to typify a instrument of measure.

Associated with range:

- Range: Interval of values of the measured variable among higher and lower limit of the measure capacity of the measurement system.
- Span: Algebraic difference between the higher and lower value of the range.
- Dead zone: Zone where the input does not makes change the output measurement value. So, does not produce reaction.

Associated with detail:

- Accuracy: Is the degree of conformity of a measured calculated quantity to its actual (true) value.
- Precision: Is the degree to which further measurements or calculations show the same or similar result. The results of calculations or a measurement can be accurate but not precise; precise but not accurate; neither; or both. A result is called valid if it is both accurate and precise.
- Sensitivity: Is the study of how output varies with changes in inputs. The element of measure is said to be sensitive to an input if changing that input variable changes the model output. This output variability (numerical or otherwise) can be apportioned, qualitatively or quantitatively, to different sources of variation in the inputs.

- Resolution: Is the level of detail that the measurement system is able to read.

Associated with reaction:

- Linearity: A measurement system is linear if the relation between the input x and the output y follows the function $y=k(x-x_0)$ where k and x_0 are constants. As much linear would be the measurement system more easier will be to calibrate it.

- Saturation: Zone where the measurement system has overtaken the maximum operation range, thereby presents an unconfident behavior.

- Hysteresis: At a given input, the output is different if we reach it increasing the input or decreasing it. We can't predict the output without looking at the history of the input. In order to predict the output, we must look at the path that the input followed before it reached its current value. A system with hysteresis has memory.

The fact that we want to study the effect of Reynolds number over the pressure coefficients and the possible hysteresis that could appears, obligate us to know which is the hysteresis inherent at measurement system, if it exists, to correct the obtained measurements.

4.1.1 Nulling technique

Probes can operate in two manners, in nulling or non-nulling technique. Nulling is a technique where the probe is always perfectly oriented and aligned at the axis parallel

to the flow. In this position the central hole measure approximately the stagnation pressure. In three-hole probes, the pressure sensed by the lateral holes theoretically must be equal. But in fact, slight differences due to manufacturing imperfections or variability of the flow field are usually observed. If the probe is measuring a two-dimensional flow field and the pressure sensed by the lateral holes are meaningfully different, it means that exist an angle among the X-axis of the probe and the velocity vector, which is defined as a yaw angle.

Non-nulling technique, or also called stationary method, gives the solution at this situation through the calibration curves yield by the experimental calibration. This permits to find out the velocity vector of the flow field interpolating the measured pressures into the calibration curves. The main advantage of this method is its simplicity which is very important in turbomachinery. On the other hand, nulling technique provides a more accurate and precise measures but needs a device that null the probe continuously. This device is governed by the pressure difference of the outer holes, moving the probe in order to find a position where the pressure difference become zero. Depending of the time of response of this device and the data acquisition system it can take long time to find out the nulling position, which makes this technique not practical for applications with high variability of the flow field direction.

Calibrate the probes over a range of yaw angles is not the objective of this work. Therefore, all the experiments are performed under nulling conditions.

4.1.2 Definition of the coefficients

The Navier-Stokes equations describe the motion of fluid substances such as liquids and gases. They ara a set of differential and non linear ecuations that may be used to model weather, ocean currents, water flow in a pipe, flow around an airfoil, and motion of stars inside a galaxy, and in general, for any phenomenon with any kind of fluid. These equations are obtained employing conservation of the mass and momentum.

The vast majority of work on the Navier-Stokes equations is done under an incompressible flow assumption for Newtonian fluids. The incompressible flow assumption typically holds well even when dealing with a "compressible" fluid, such as air at room temperature (even when flowing up to about Mach 0.3). Taking the incompressible flow assumption into account and assuming constant viscosity, the Navier-Stokes equations will read (in vector form)

$$\rho\left(\frac{\partial w}{\partial t} + w \cdot \nabla w\right) = -\nabla p + \mu \nabla^2 w + f \tag{4.1}$$

A solution of the Navier-Stokes equations is called a velocity field or flow field, which is a description of the velocity of the fluid at a given point in space and time. Once the velocity field is solved for, other quantities of interest (such as flow rate, drag force, or the path a "particle" of fluid will take) may be found. There are analytic solutions only for very concrete situations. For the rest of situations, numerical analysis is needed to solve the equations. The branch occupied to solve it is called *Computational Fluid Dynamics*. The formulation employed in this work is so much simple than the equation of Navier-Stokes, because we assume a set of simplifying

hypothesis which facilitates its solution. Actually the degree of precision needed for this work does not make practical to use CFD.

Under the assumption that the flow field provided by the wind tunnel is an one-dimensional steady flow. The turbulence is supposed very low, the characteristics of the wind tunnel say that is approximately 1%, so it can be considered as negligible. These simplifications drops out many terms of the Eq.(4.1). As a result, it is obtained the Bernouilli conservation equation, which states that stagnation pressure is the sum of static pressure and dynamic pressure,

$$p + \frac{1}{2}\rho w^2 = const \tag{4.2}$$

The dynamic pressure is the second term of the above equation and represents fluid kinetic energy. Static pressure p is not associated with the fluid motion but rather with its state. The velocity is not a parameter which can be measured with a probe, but it can be calculated from the measurements of the total and static pressure.

$$w = \sqrt{\frac{p_t - p}{\rho/2}} \tag{4.3}$$

Reynolds number is a non-dimensional parameter widely used in fluid motion. It expresses relation between inertial and viscous forces of the flow, useful to identify the flow regime.

$$Re_d = \frac{wd}{\nu} \tag{4.4}$$

The subscript d indicate that it is calculated with the characteristic diameter of the probe, which is the probe width.

Mach number allows to assume that one gas at low velocity can be considered as incompressible.

$$Ma = \frac{w}{w_0} \tag{4.5}$$

Treaster and Yocum coefficients

The pressure sensed by the hole is measured as the moving air brought to rest. For each hole the pressure can be expressed as a non-dimensional pressure coefficient as the following formula.

$$k_i = \frac{p_i - p}{\frac{\rho}{2} w^2} \tag{4.6}$$

where i identify the hole of the probe.

The hole pressure coefficients are used to reduce the data on the non-dimensional coefficients defined by Treaster and Yocum [8].

Direction coefficient,

$$k_\beta = \frac{p_2 - p_3}{p_1 - \bar{p}} = \frac{k_2 - k_3}{k_1 - \bar{k}} \tag{4.7}$$

Total pressure coefficient,

$$k_t = \frac{p_1 - p_t}{p_1 - \bar{p}} = \frac{k_1 - 1}{k_1 - \bar{k}} \tag{4.8}$$

Static pressure coefficient,

$$k_s = \frac{\bar{p} - p}{p_1 - \bar{p}} = \frac{\bar{k}}{k_1 - \bar{k}} \tag{4.9}$$

Dynamic pressure coefficient was not defined by Treaster and Yocum, it was defined by the manufacturer of SVUSS/3 cobra probe. It is used in this work in order

to compare our results with the calibration data supplied by them.

$$k_d = \frac{p_t - p}{p_1 - p_2} = \frac{1}{k_1 - k_2} \tag{4.10}$$

where,

$$\bar{p} = \frac{p_2 + p_3}{2} \tag{4.11}$$

$$\bar{k} = \frac{k_2 + k_3}{2} \tag{4.12}$$

4.2 Streamline Projection Method

The streamline is a curve everywhere tangent to the instantaneous velocity vector of the flow. It means that velocity vector has at each point the same direction as the streamline. The streamline projection method is only valid under the hypothesis that the free stream velocity is projected directly on each one of the three sensing holes, with the assumption that the velocity magnitude is constant. In this situation the holes are sensing the free stream static pressure in addition at the dynamic pressure which velocity component is normal at them. This means that the holes of the probe are measuring the total pressure as a sum of static and dynamic pressure. The sreamline projection method can also be used for an approximation of the influence of a velocity gradient [10] as well to find out the influence of a wall proximity effect [9] which can be interpreted such a flow angle error. But these applications are not the aim of this work.

The mathematical formulation is the following,

$$p_i = p + \frac{1}{2}\rho w_i^2 \tag{4.13}$$

where the subscript i refers to the subject pressure. Employing the equations that defines the hole calibration coefficients we obtain,

$$p_i = p + \frac{k_i}{2}\rho w_i^2 \tag{4.14}$$

Then we can rewrite the hole coefficient as a combination of Eq.(4.13) and (4.14).

$$k_i = \left(\frac{w_i}{w}\right)^2 \tag{4.15}$$

All restrictions of this method above explained, makes that streamline projection method could be considered as a purely geometrical method, due to the probe head geometry is the only parameter dependant. But it is a quite good and easy way to estimate the hole coefficients analytically.

The three probes used in this work, even though they have different head dimensions, there are only two different shapes of the sensing forward area, trapezoidal and cylinder. Hence the streamline projection equations will be different not for each probe, but rather for each shape of the head.

Next step is applying the streamline equations to deduce the pressure sensed by the holes, decomposing the velocity vector in the normal direction at each hole of every probe head geometry.

4.2.1 Trapezoidal head

As is it said before, SVUSS/3 cobra probe and AVA 110 trapezoidal probe have the same characteristic wedge angle $\delta = 30°$, thus for this sort of head probe the streamline equations are valid for both.

Fig.4.1 shows how the projections of velocity vector are done into normal direction of each hole,

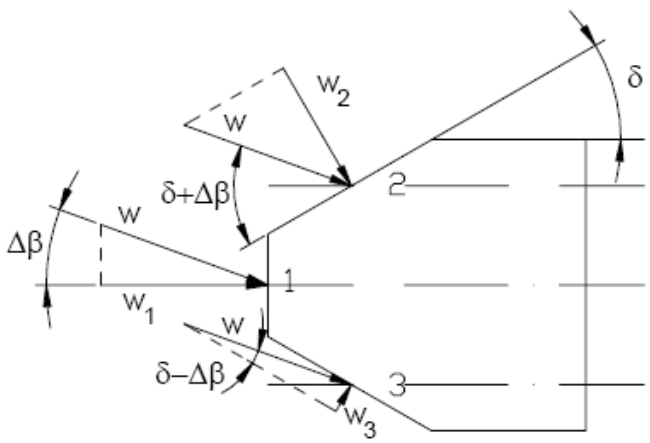

Figure 4.1: Descomposed velocities over trapezoidal probe head

$$w_1 = w \cos \Delta\beta \tag{4.16}$$

$$w_2 = w \sin (\delta + \Delta\beta) \tag{4.17}$$

$$w_3 = w \sin (\delta - \Delta\beta) \tag{4.18}$$

Replacing the above equations at hole pressure formula, we obtain the pressure sensed by the holes,

$$p_1 = p + \frac{1}{2}\rho \left(w \cos \Delta\beta\right)^2 \tag{4.19}$$

$$p_2 = p + \frac{1}{2}\rho \left[w \sin (\delta + \Delta\beta)\right]^2 \tag{4.20}$$

$$p_3 = p + \frac{1}{2}\rho \left[w \sin (\delta - \Delta\beta)\right]^2 \tag{4.21}$$

The hole coefficients are,

$$k_1 = \cos^2 \Delta\beta \tag{4.22}$$

$$k_2 = \sin^2 (\delta + \Delta\beta) \tag{4.23}$$

$$k_3 = \sin^2 (\delta - \Delta\beta) \tag{4.24}$$

As it is showed at the above equations, the holes coefficients are only dependent of geometric parameters such as yaw angle as well as on the wedge angle of the probe's head. These also can be used to calculate the direction, total, static and dynamic pressure coefficients at Eq.(4.7), Eq.(4.8), Eq.(4.9) and Eq.(7.1) respectively.

4.2.2 Cylinder head

The procedure to fit the streamline projection equations is basically the same, the difference of head geometry introduce some changes into projections of velocity vector components as shows Fig.4.2.

The velocity components into normal direction of each hole are,

$$w_1 = w \cos \Delta\beta \tag{4.25}$$

$$w_2 = w \cos (\delta - \Delta\beta) \tag{4.26}$$

$$w_3 = w \cos (\delta + \Delta\beta) \tag{4.27}$$

The pressures sensed by the holes, are obtained replacing the above velocities into pressure equations,

$$p_1 = p + \frac{1}{2}\rho \left(w \cos \Delta\beta\right)^2 \tag{4.28}$$

$$p_2 = p + \frac{1}{2}\rho \left[w \cos (\delta - \Delta\beta)\right]^2 \tag{4.29}$$

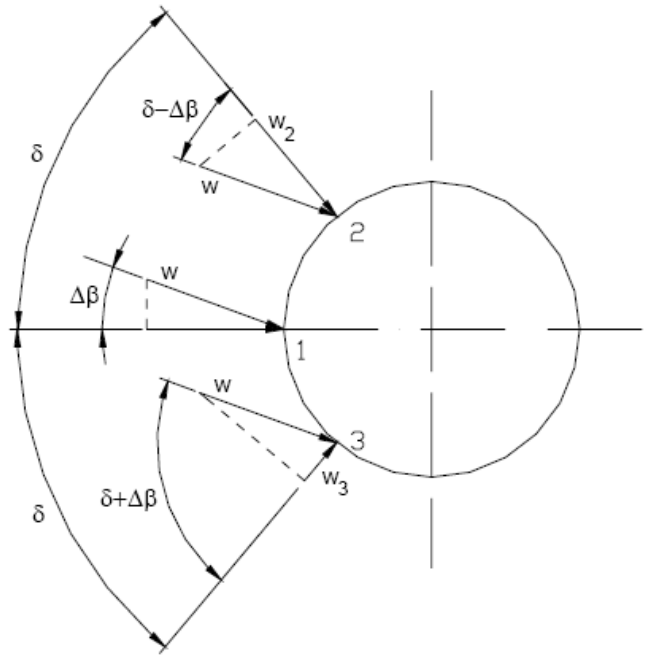

Figure 4.2: Descomposed velocities over cylinder probe head

$$p_3 = p + \frac{1}{2}\rho \left[w \cos\left(\delta + \Delta\beta\right)\right]^2 \tag{4.30}$$

And finally the hole coefficients are calculated applying the above pressure equations into Eq.(4.6),

$$k_1 = \cos^2 \Delta\beta \tag{4.31}$$

$$k_2 = \cos^2 \left(\delta - \Delta\beta\right) \tag{4.32}$$

$$k_3 = \cos^2 \left(\delta + \Delta\beta\right) \tag{4.33}$$

4.3 Potential flow

Potential flow is well known and widely explained in many books of fluid mechanics. Is characterized by an irrotational velocity field. This property allows the description

of the velocity field as the gradient of a scalar function as equation below also called Laplace's equation,

$$\nabla^2 \Phi = 0 \tag{4.34}$$

This equation can be used to calculate solutions to many practical flow situations. Potential flow does not include all the characteristics of flows that are encountered in the real world. For example, potential flow excludes turbulence, which is commonly encountered in nature.

From potential flow are obtained lines of constant ψ that are known as streamlines and lines of constant φ known as equipotential lines. Equipotentials are lines of equal head that are in direct relation to pressure. Streamlines are perpendicular to the equipotentials and have the same direction of the flow.

The result of applying this theory of potential flow around a cylinder is the below equation,

$$k_i = \frac{p(\varphi) - p}{\frac{1}{2}\rho w^2} = 1 - 4\sin^2\varphi \tag{4.35}$$

where the angle φ is measured between flow direction and the cylinder radius that goes across the hole i. Considering the geometry of the cylinder head probe, the Eq.4.35 becomes the following expression for each hole.

$$k_1 = 1 - 4\sin^2 \Delta\beta \tag{4.36}$$

$$k_2 = 1 - 4\sin^2 (\delta - \Delta\beta) \tag{4.37}$$

$$k_3 = 1 - 4\sin^2 (\delta + \Delta\beta) \tag{4.38}$$

The hole coefficients of both methods can be also used to calculate the nondimensional coefficients defined by Treaster and Yocum.

4.4 Calibration Procedure

The calibration procedure is the same for the three probes. The calibration is done within a range of velocities between 19 up to 78m/s. Mach number is always lower than 0.3 which allows assuming that the fluid is incompressible. Actually the highest Mach numer reached is 0.23, so this assumption can be done without introduce error at the measures.

The probes are mounted in a support device, which permit to modify the pitch and yaw angle. The probe tips are at 130mm downstream from the nozzle exit and far enough from the base of subjection to avoid interference effects.
Since the probe is placed at the core of the flow at a downstream distance from the nozzle exit lower than 2.5 times the nozzle diameter, a homogeneous flow field is expected.

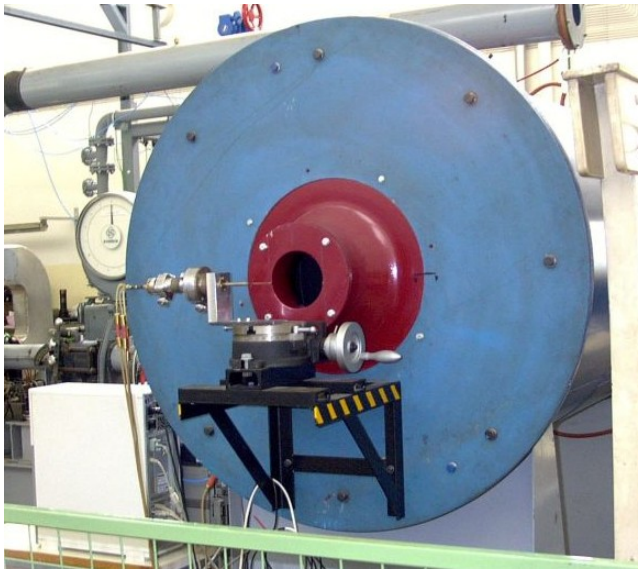

Figure 4.3: Nozzle exit of the wind tunnel

Before to start to perform the calibration, the probes were nulled manually. The holes 2 and 3 were connected to a tube in U with water in its interior to measure the differential pressure. The probe was placed at the support device and subjected to an air flow supplied by the wind tunnel. It amended the angle yaw until the water level of the two tubes was the same, which means that the pressure of the two side holes is the same, therefore the probe is in nulling position.

Once the probes were nulled, the calibration starts setting the motor velocity at 400rpm. We take the measures and the next step is increase the motor velocity 50rpm. The measures are taken again and the same procedure is done until reach 1600rpm. Then it is followed the inverse sequence, the velocity of the motor is decreased in steps of 50rpm until 600rpm taking measures at each step. The parameters measured were the following:

- Flow temperature, T
- Hole pressures p_1, p_2, p_3
- Total flow pressure p_t

We take 30 single measures for each parameter during an interval of 0.2 seconds. These measures are treated by LabVIEW, which through a data reduction program calculates the mean of each parameter. Employing the measured data, the program generates an output file with the following parameters, needed to evaluate and calibrate the probes:

- Flow velocity w

- Mach number Ma
- Reynolds number Re_d
- Hole coefficients k_i
- Direction coefficient k_β
- Total pressure coefficient k_t
- Static pressure coefficient k_s
- Dynamic pressure coefficient k_d

These parameters are calculated with the equations explained at the section 4.1.2, called *Definition of the coefficients*.

Chapter 5

Test Facility

The experimental calibration of the three-hole probes has been carried out at the laboratory of the Institute of Thermodynamics and Energy Conversion of the University of Technology of Vienna.

The main equipment employed consists in a free jet wind tunnel, the three-hole probes with different head geometries and the data acquisition system. The characteristics of the probes were already described at Chapter 3.

The characteristics of the wind tunnel and the data acquisition system are described below.

5.1 Wind Tunnel

A free jet wind tunnel is used for the probes calibration at different Reynolds numbers. The velocity of the flow field is fixed manually using the transmission for speed control which actuates on a 50kW DC motor. The motor drives a radial blower of 1115mm in diameter, and it is able to supply $3m^3/s$ airflow.

To avoid the high level of turbulence, the wind tunnel is equipped with nylon screens placed upstream of the nozzle inlet. The objective is to obtain a homogenous flow field downstream of the nozzle exit, thus it is possible to approximate that, under nulling conditions, all holes are sensing the same X-axis velocity. The stream wise turbulence intensity is about 1%. The throat diameter of the convergent nozzle exit is 120mm and the probe head is mounted in a subjection structure at 130mm downstream of the nozzle exit plane.

At the exit throat, there is a ring with 8 pressure sensors connected among them to measure the total pressure at the exit of the wind tunnel. Also a Pt-100 resistor thermometer, placed inside the wind tunnel, is used to measure the flow temperature.

The main technical characteristics of the free jet wind tunnel are summarized in Table 5.1.

Characteristic	Value
Power supply	$50kW$ DC motor
Flow rate	$3m^3/s$
Nozzle diameter	$120mm$
Contraction ratio	1:69.4
Diffuser divergence	5.7°
Mach number	0.05 - 0.3
Reynolds number	variable
Turbulence intensity	$\approx 1\%$

Table 5.1: Technical data of the wind tunnel

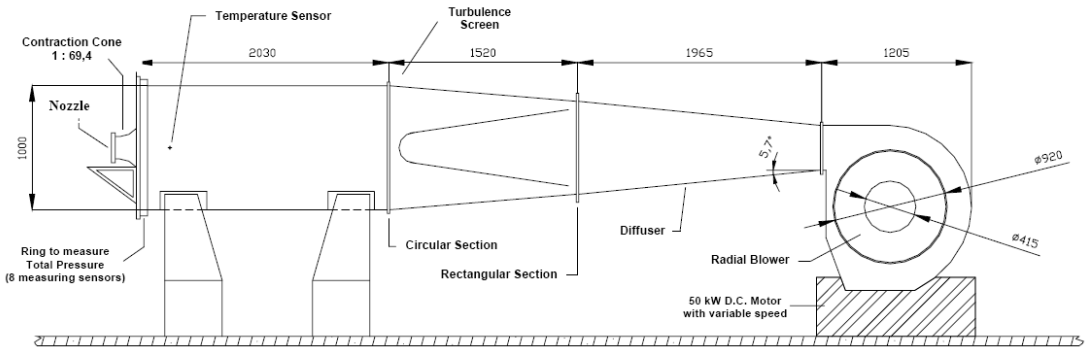

Figure 5.1: Sketch of the wind tunnel

5.2 Data Acquisition System

The three-hole probes, as are defined at 3th chapter, are the medium for what the sensed pressures at the head are driven through the tubes until the transducer. The transducer is the element which measures quantitatively the pressure. Thus, is important to characterize the transducer.

The pressures are converted into electrical signals through a piezoresistive transducer. The operation system of a piezoresistive pressure transducer consist of flexible diaphragms also called piezoelectric elements with a crystalline substance between those that generates a voltage difference when is subject of mechanical deformations.

The piezoresistive pressure transducers is powered with 8V DC set manually with an accuracy of $\pm 1mV$. Since the measured pressures are relative to the atmospheric, these can be positive or negative. The piezoresistive transducer used is DA 27, 186PC03D. Fig.5.2 shows the behavior of the transducer.

A perfect linear relation over entire range is observed, which can be expressed

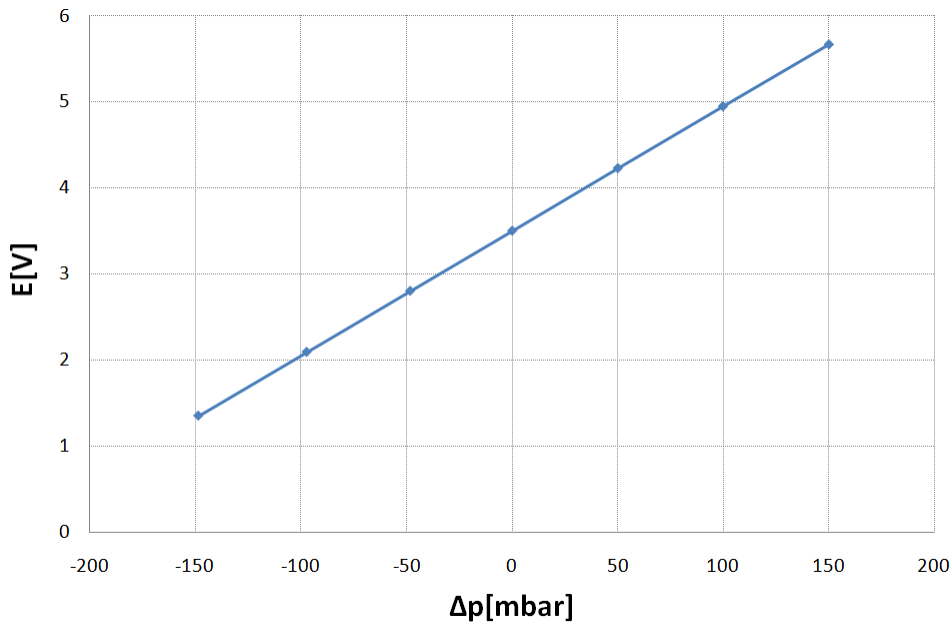

Figure 5.2: Transducer graph conversion

mathematically as the next formula. The units are [mbar] and [V], therefore the conversion from pressure to voltage is immediate.

$$E = 0.014\Delta p + 3.502 \tag{5.1}$$

A summary of the characteristics of the transducer can be found in Table 5.2.

Parameter	Value
Type	Piezoresistive
Range	$\pm 172 mbar$
Span	$344 mbar$
Dead zone	$\leq -172 mbar \& \geq 172 mbar$
Linearity	Yes

Table 5.2: Transducer data DA 27, 186PC03D

All data is recorded by HP 3852A acquisition system, which is connected to PC via GPIB bus, where LabVIEW software makes the adequate data treatment.

Chapter 6

Results and Discussion

In this chapter are evaluated the results obtained by the experiment made at the facilities, following the procedure described at the Chapter 4. A complete set of data is obtained for each probe. In order to make easier compare the results and the behavior of the probes with the same head geometry, trapezoidal head, it is used the same scale to plot the same coefficients. Adapting the scale at the values for each coefficient but being the same for both probes.

The comments of the plots are also evaluated into a sorted and sequential form. Presenting and analyzing firstly the hole coefficients, and afterwards the direction, the total pressure, the static and the dynamic pressure coefficients, in this order. Following the aim of this work, the coefficients are plotted versus the Reynolds number. A special emphasis is done into the analysis of the differences that could appear between the measures obtained while the velocity of the flow field increase respect the obtained ones while the velocity decrease.

The coefficients calculated for each probe are also compared with the values cal-

culated with streamline projection method. In the case of the AVA 43 cylinder probe the potential flow solution has been also studied. Both methods have been explained previously at Chapter 4. The values that these methods provide are showed at the Table 6.1.

	Trapezoidal head	Cylinder head	
Coefficient	Streamline[-]	Streamline[-]	Potential flow[-]
k_1	1	1	1
k_2	0.25	0.413	-1.347
k_3	0.25	0.413	-1.347
k_β	0	0	0
k_t	0	0	0
k_s	0.333	0.704	-0.574
k_d	1.333	1.704	0.426

Table 6.1: Coefficients calculated analytically

6.1 SVUSS/3 Cobra Probe

The environment conditions under which the experiment was developed are the follows:

- $T = 16.5°$C, being 21.0°C the maximum temperature reached.
- $p_a = 1002.6$mbar of atmospheric pressure.
- Probe placed at the core of the flow field, 130mm downstream of the nozzle exit and nulled manually. However the indicator marks $-1.5°$ of yaw angle.
- Probe diameter = 2.4mm.
- Range of Reynolds number = 3000 up to 12000.

As it was expected, the value of k_1 does not show any type of variation in relation over the entire Reynolds number. It keeps constant in all the range. Due to for its own definition in Eq.(4.22) the numerator and the denominator rise insofar that the velocity of the flow field as well it does. The graph shows perfect consonance with the value calculated using streamline projection method $k_1 = 1$. Differences between increasing and decreasing the flow velocity are not appreciated.

The coefficients of the two lateral holes of SVUSS/3 probe present a similar behavior. Both show a progressive decreasing trend at relatively low Reynolds numbers until stabilizes between 7000 and 8000. From there, the value of the coefficients is maintained more or less constant. This value approaches with quite good precision at the value calculated by streamline projection method where $k_2 = k_3 = 0.25$.

However, the trend showed by k_3 is much clear than the trend of k_2 which has more dispersion and some values are very far of the trend line. The region with highest degree of scatter is among 8000 and 10000 Reynolds number.

Naturally the direction coefficient in nulled position must be zero, as it is calculated through streamline projection method $k_\beta = 0$. Even though k_β is calculated with the mean of k_2 and k_3, the error that introduce the deviation of the hole coefficient k_2 respect the main trend generates a slight deviation of the direction coefficient at low Reynolds numbers observed at the graph.

Total pressure coefficient presents almost the same comportment as the hole coefficient number one k_1. Due to the probe is nulled k_1 senses the stagnation pressure. Although both plots are very similar, the most significant difference is the value being $k_t = 0$ instead of 1, in concordance with the streamline projection method.

Static pressure coefficient is the parameter that presents a more clear variation with Reynolds number. The trend is basically the average of the values of the outer holes coefficients as its formula implies. A deviation of the expected trend is observed on the Reynolds number among 7000 and 9000, which modifies the normal trend drawing a strange hill to finally reach the expected trend again. These anomalies are observed for the increasing and also for the decreasing of the Reynolds number. Is the only paramether that shows a possible hysteresis behavior.

Under nulled position, which means that $k_1 \approx 1$ and for its own definition makes that the dynamic pressure coefficient is dependent only of k_2. This fact explain why the plot of k_d is pretty like as the plot of k_2, with the same degree and location of the scatter.

An additional graph of dynamic pressure coefficient is included in order to compare the experimental results and the calibration data provided by the manufacturer. One realizes that the behavior shown by k_s is very similar at that k_d of the manufacturer shows. If both coefficients are analyzed numerically employing the streamline projection equations, taking into consideration that the experiment is under nulling conditions and $\Delta\beta = 0$, it is easy to find the relation between them,

$$k_s = tan^2\delta = \frac{sin^2\delta}{cos^2\delta} = \frac{1 - cos^2\delta}{cos^2\delta} \tag{6.1}$$

And the value of k_d for streamline projection method is,

$$k_d = \frac{1}{cos^2\delta} \tag{6.2}$$

Thus, if we combine the above equations we find,

$$k_d = 1 + k_s \tag{6.3}$$

Thus, due to the great dispersion shown by k_d. To contrast the results with greater clarity, it considers appropriate to present in the same graphic k_d (manuf.) and $k_s + 1$ (exp.). As it can be observed, the calibration data of the manufacturer cover a larger range of Reynolds number than the obtained carrying out the experiment. This fact is due to the technical limitations of the speed-control system of the motor that made

impossible to work giving a homogenous and stable airflow at velocities lower than 400rpm.

Both curves present exactly the same shape and trend, with a located zone that could be interpreted as hysteresis. However, a curiously is observed, both curves are horizontally separated for 20m/s.

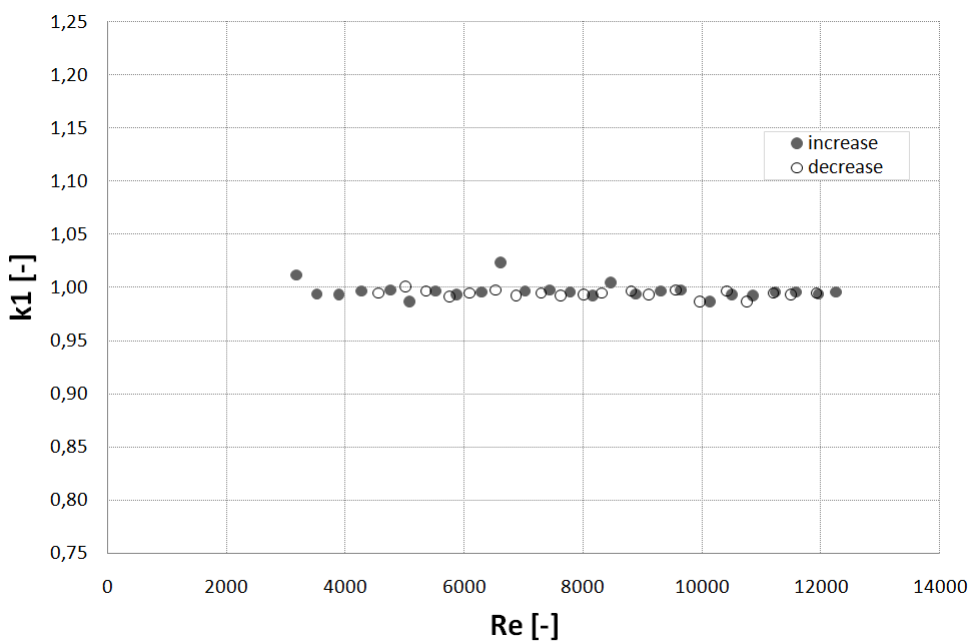

Figure 6.1: SVUSS/3 cobra probe hole coefficient k_1

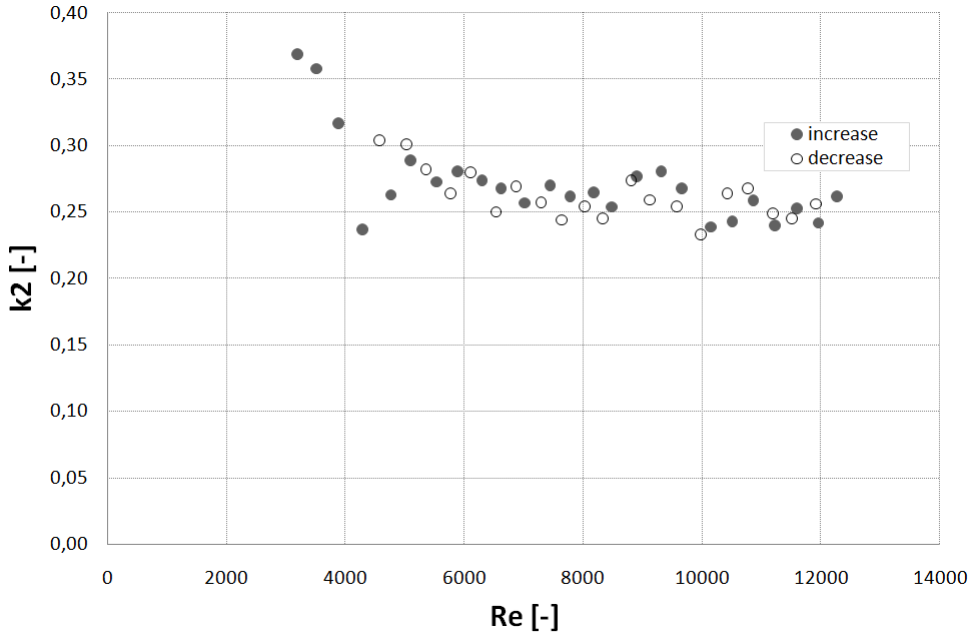

Figure 6.2: SVUSS/3 cobra probe hole coefficient k_2

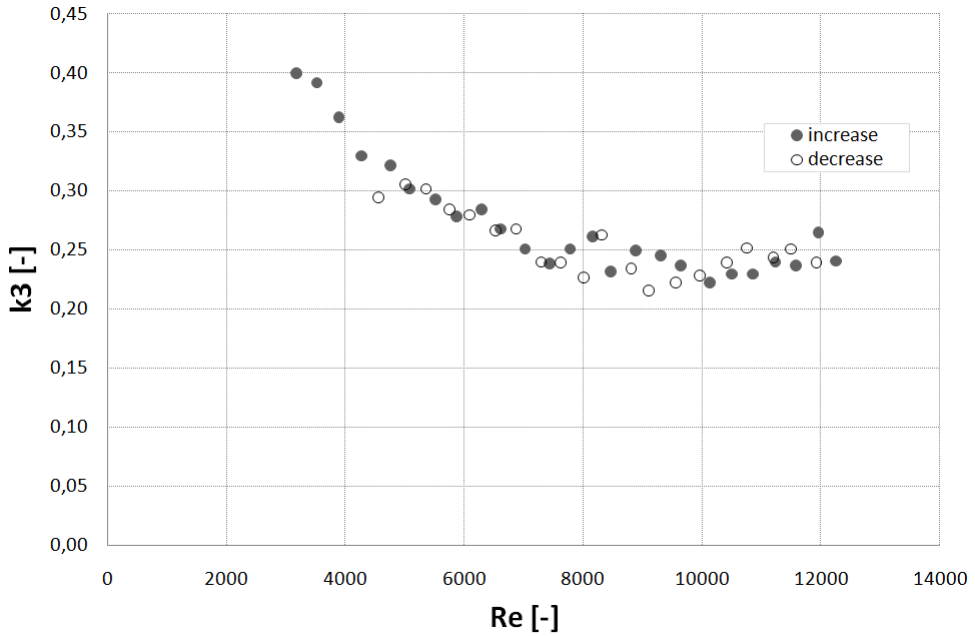

Figure 6.3: SVUSS/3 cobra probe hole coefficient k_3

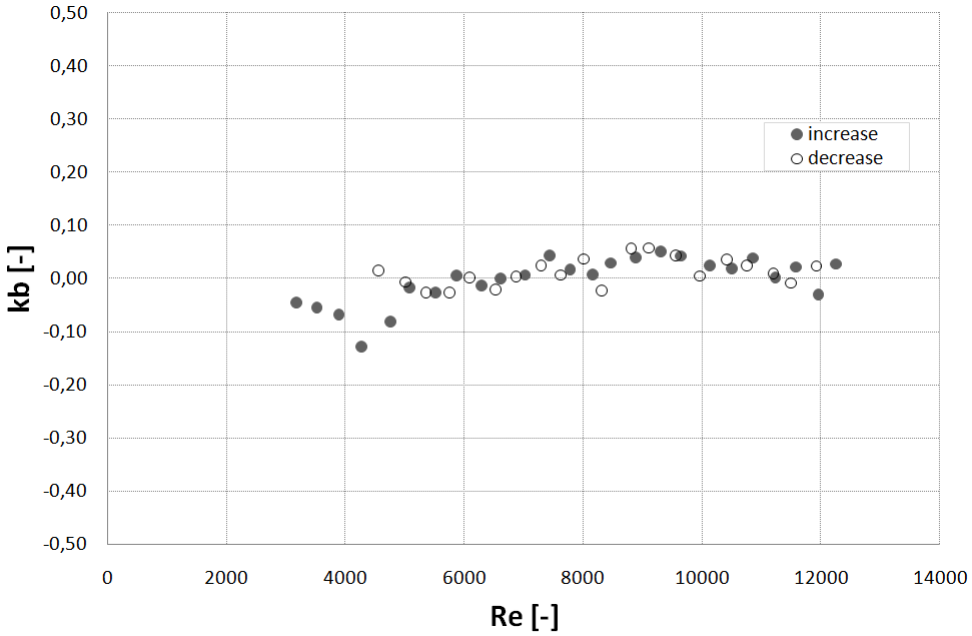

Figure 6.4: SVUSS/3 cobra probe direction coefficient k_β

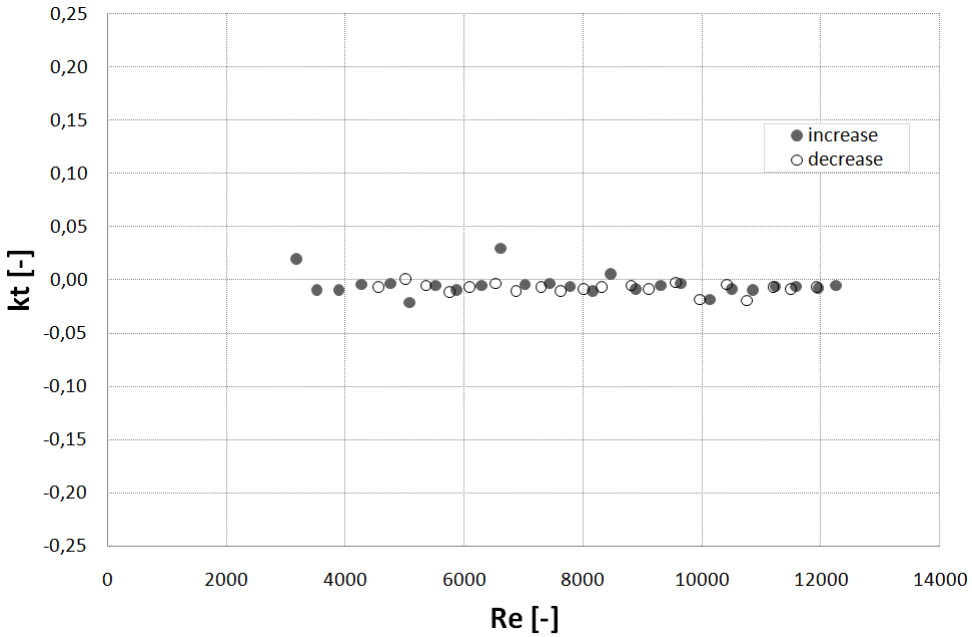

Figure 6.5: SVUSS/3 cobra probe total pressure coefficient k_t

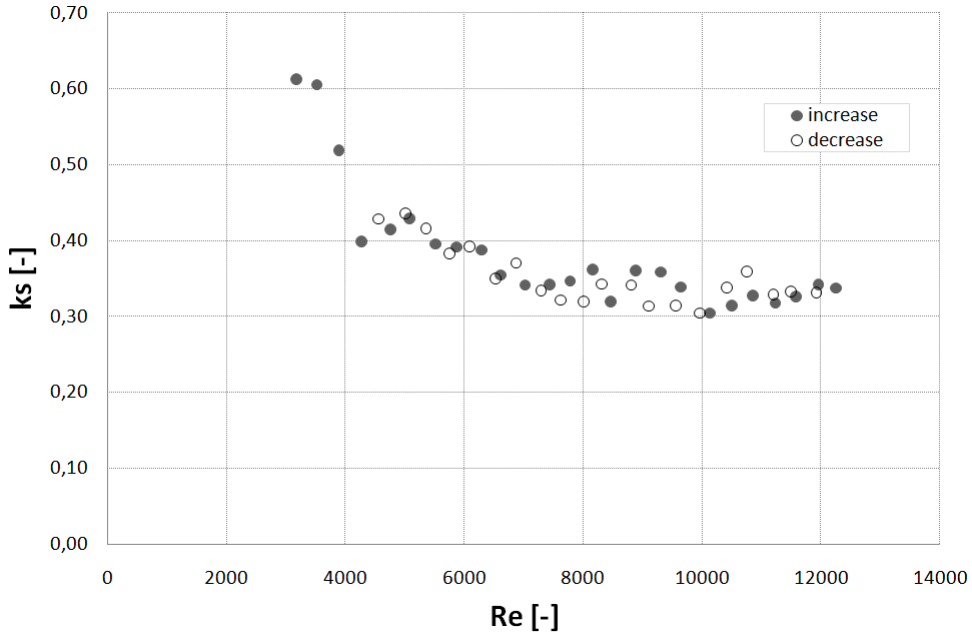

Figure 6.6: SVUSS/3 cobra probe static pressure coefficient k_s

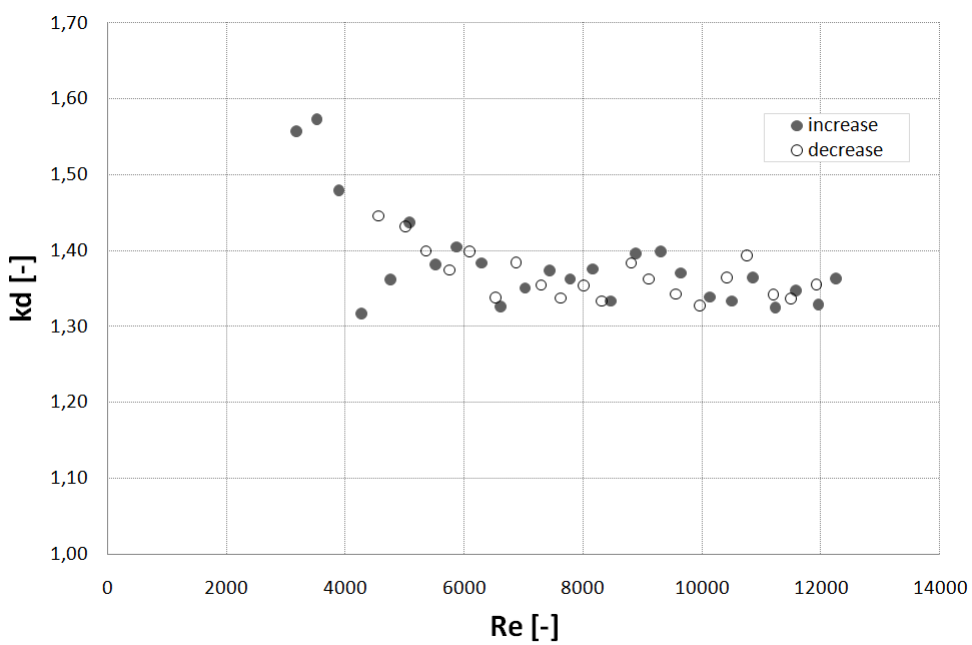

Figure 6.7: SVUSS/3 cobra probe dynamic pressure coefficient k_d

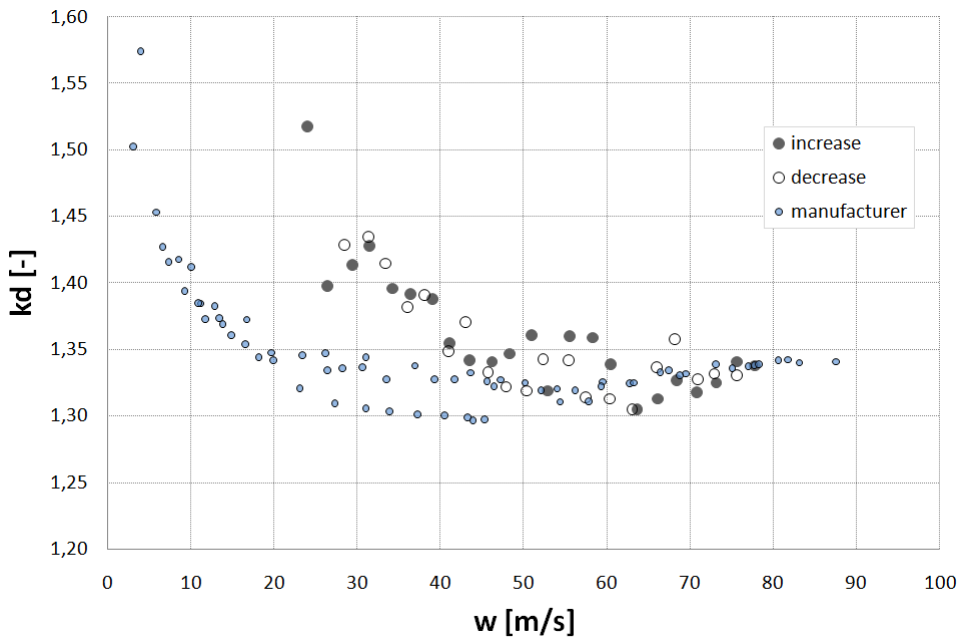

Figure 6.8: Adapted k_d as $k_s + 1$ in comparison with k_d of manufacturer data

6.2 AVA 110 trapezoidal probe

The environment conditions under which the experiment was developed are the follows:

- $T = 17.3°$C, being 22.1°C the maximum temperature reached.
- $p_a = 1002.4$mbar of atmospheric pressure.
- Probe placed at the core of the flow field, at 130mm downstream of the nozzle exit and nulled manually. However, the indicator marks $-2.5°$ of yaw angle.
- Probe diameter = 3.3mm.
- Range of Reynolds number = 4500 up to 17500.

It is easily imaginable that two probes with the same head geometry, under the same work conditions, will present similar behavior. As it is mentioned at the chapter where the geometries of the probes are described, SVUSS/3 and AVA 110 have the same trapezoidal head geometry with the same characteristic wedge angle. This fact allows compare the results of both probes, and in function of those choose the proper probe for a concrete application. The most meaningful difference between the plots of the two probes is not the slope or the trend of the curves, because as it can be checked are pretty much the same at the shown by SVUSS/3, it is the lateral movement in the values for the X-axis for the Reynolds number. This fact is due to, even though the velocities range that are the probe exposed is the same, the Reynolds number is a non-dimensional parameter calculated with the characteristic diameter of the probe, Eq.(4.4). As the characteristic diameter of the AVA 110 trapezoidal probe is 3.3mm instead of 2.4mm of the SVUSS/3 cobra probe, it generates this lateral displacement of 2000 units approximately. Being now the range of Reynolds number between 4000 and 17000. This difference was not observed if the graphics were submitted as the evolution of any coefficient versus the velocity of the flow expressed in meters per second. Due to the velocities range for all the probes of this work are approximately between 20 and 80m/s.

The interpretation of the hole coefficients is basically the same as for SVUSS/3 cobra probe ones. k_1 is completely plane in 1, only several points are far away from the expected value. The other hole coefficiens k_2 and k_3, present a similar behavior. The curve has a decreasing slope at low Reynolds number until it stabilizes at 10000. From there, the degree of scatter increase, showing a high fluctuation of the values

until the end of the range. The average of all these points seems to be an horizontal line of value a bit higher than 0.2, but far from the calculated with streamline projection method that must be $k_2 = k_3 = 0.25$. Any of the hole coefficients show significant differences between increasing and decreasing the Reynolds number.

Direction pressure coefficient presents a moderate degree of dispersion of the measures around the value predicted by streamline projection method where $k_\beta = 0$. The argument that explains this scatter is the same that has been described for the SVUSS/3 cobra probe, if k_β is calculated with k_2 and k_3 and these show dispersion, it is logical that the direction coefficient has got it as well.

Total pressure coefficient does not show nothing special, very plane around zero. Which means that the probe is quite well nulled. But if it is looked more attentively, one can realize that most of the measures are slightly under zero. To that $p_1 - p_t$ would be negative, p_t must be bigger than p_1. Which means that there are a pressure loss from where the total pressure is measured until where the probe is placed to measure the total pressure through the hole number 1. This explanation is useful for all the probes, as it can be checked at all the k_t graphs.

Static pressure coefficient presents the same behavior than the outer hole coefficients. As it can be observed the slope of the curve follows the same trend but with the singularity that the scatter has been reduced thanks that k_s is calculated with the average of the holes 2 and 3.

There is no significant differences on the measures of k_s between increasing and de-

creasing the Reynolds number. From $Re = 10000$ the value of k_s stabilizes reaching a horitzontal curve, but appears a big fluctuation that generates a false sensation of horitzontality and stability of the measures. The average value of all these fluctuation points where k_s seems stable is points roughly comparable at the value calculated with streamline projection method $k_s = 0.33$.

The huge scatter presented by the dynamic pressure coefficient makes necessary a rethinking of a modification in the way to calculate it. As it is shown at the graphs of the two trapezoidal head probes, makes nonviable extract any conclusion far that although a high degree of dispersion and fluctuation is observed, the average value approaches relatively at the expected one for streamline projection method $k_d = 1.33$.

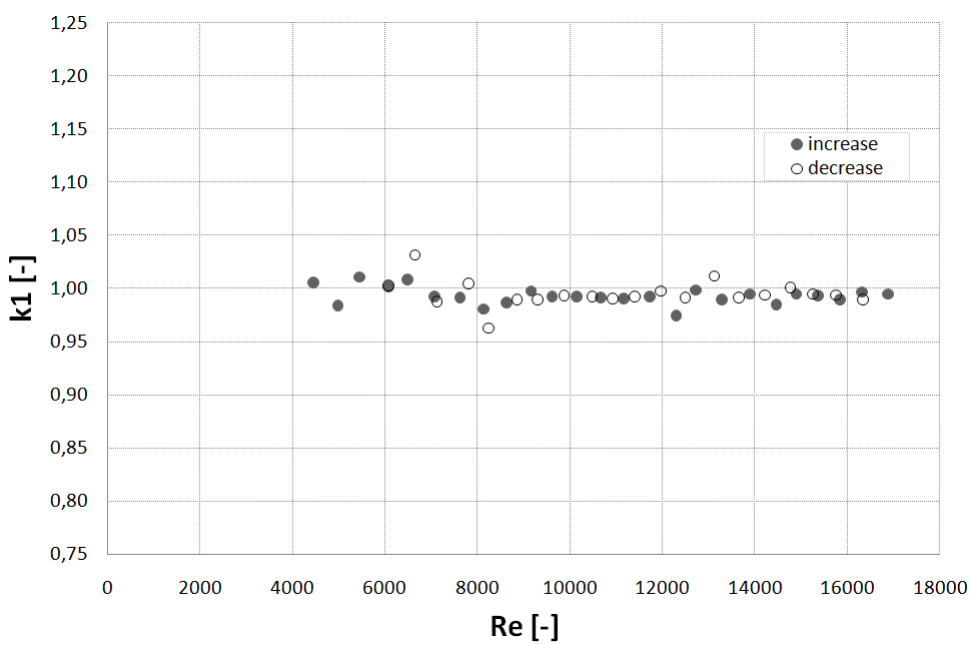

Figure 6.9: AVA 110 trapezoidal probe hole coefficient k_1

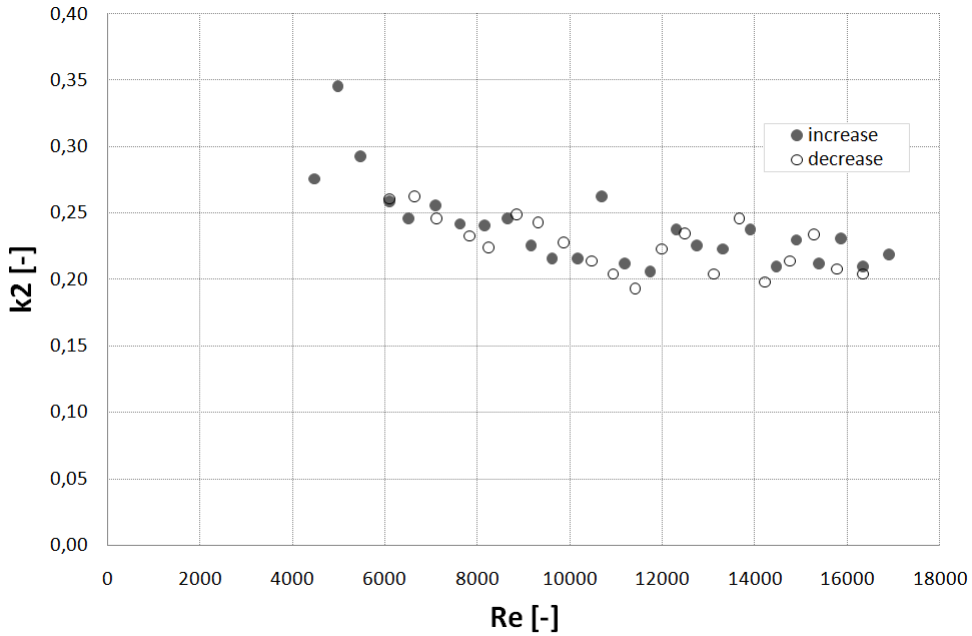

Figure 6.10: AVA 110 trapezoidal probe hole coefficient k_2

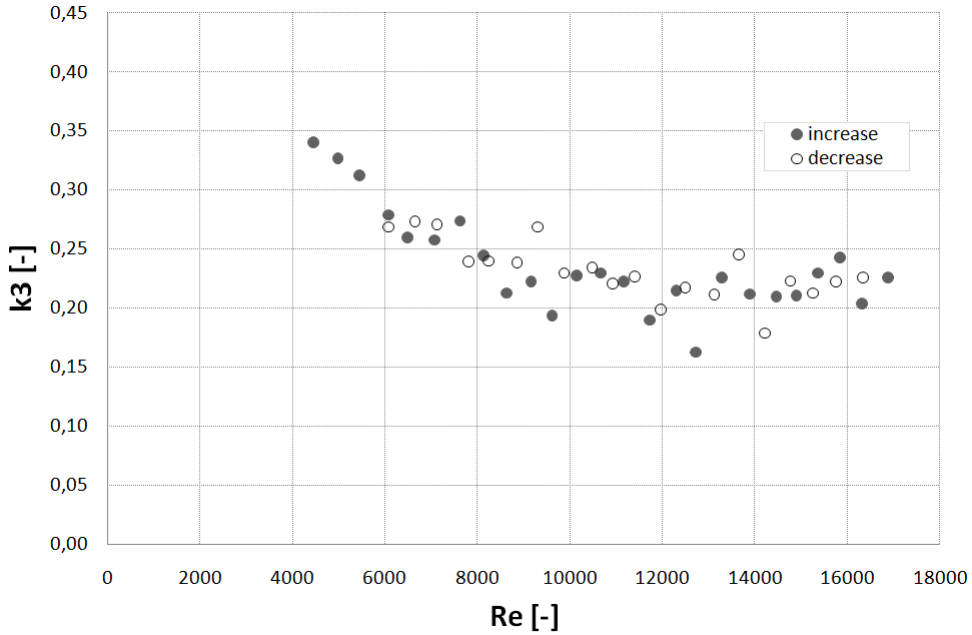

Figure 6.11: AVA 110 trapezoidal probe hole coefficient k_3

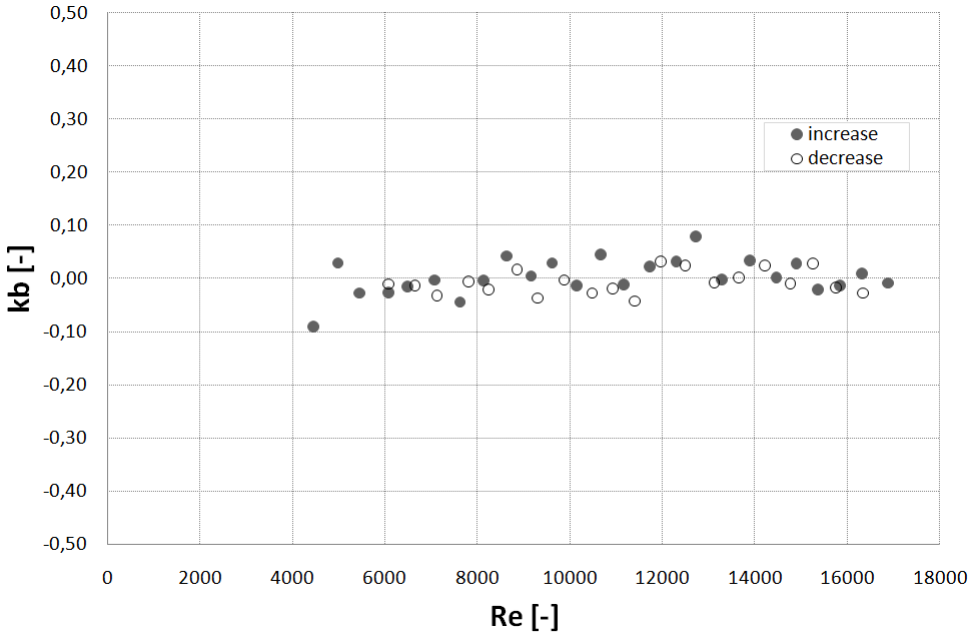

Figure 6.12: AVA 110 trapezoidal probe direction coefficient k_β

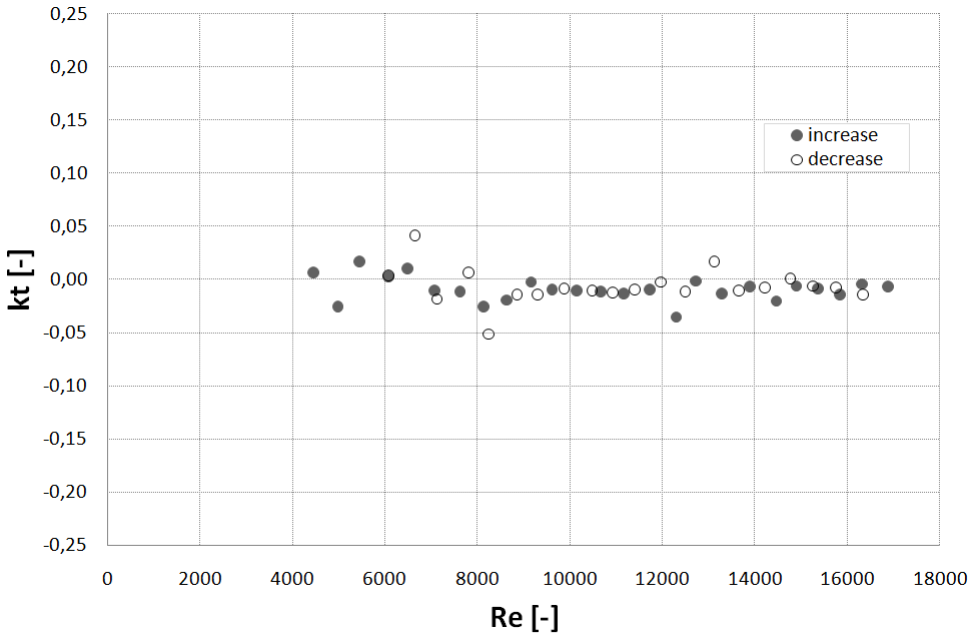

Figure 6.13: AVA 110 trapezoidal probe total pressure coefficient k_t

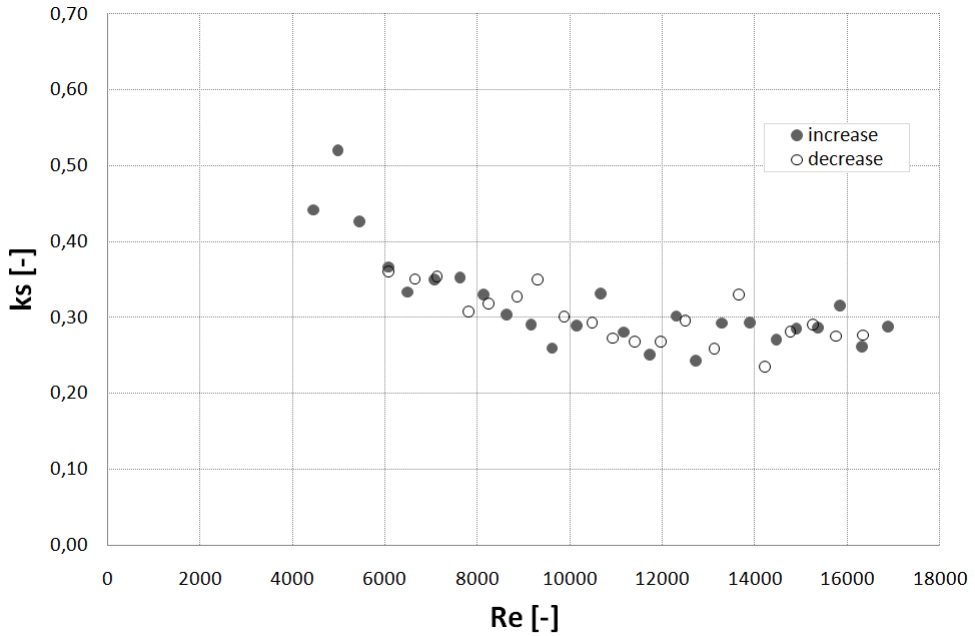

Figure 6.14: AVA 110 trapezoidal probe static pressure coefficient k_s

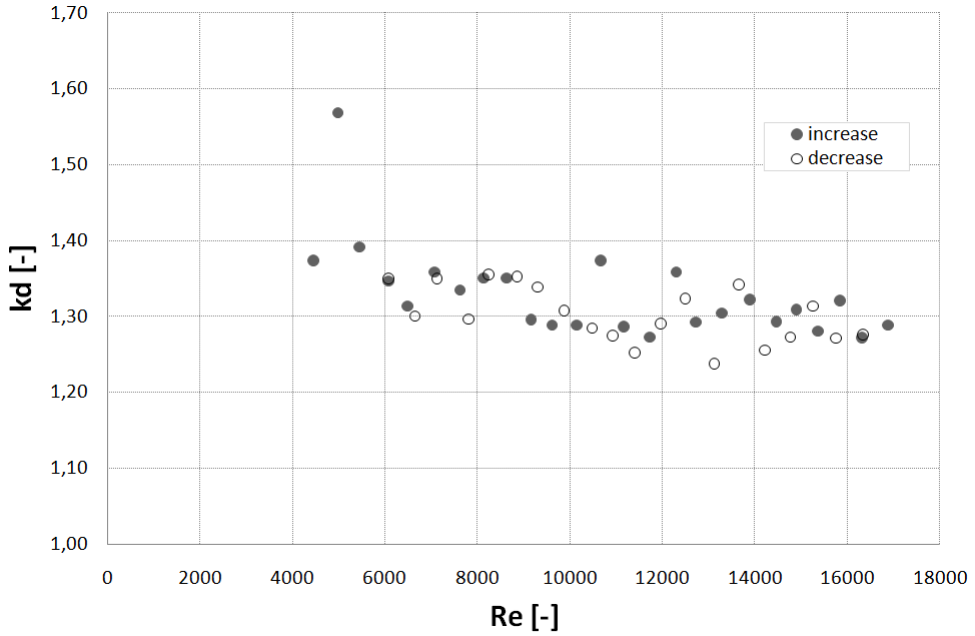

Figure 6.15: AVA 110 trapezoidal probe dynamic pressure coefficient k_d

6.3 AVA 43 cylinder probe

The environment conditions under which the experiment was developed are the follows:

- $T = 17.4°$C, being 21.3°C the maximum temperature reached.
- $P_a = 1002.5$mbar of atmospheric pressure.
- Probe placed at the core of the flow field, at 130mm downstream of the nozzle exit and nulled manually.
- Probe diameter = 3.0mm.
- Range of Reynolds number = 4000 up to 16000.

Hole coefficient k_1 does not show any deviation respect the expected behavior, all the measures are very close to $k_1 = 1$ with independence if the velocity increases or decreases. Some few points at low Reynolds number are a bit far from the mean, but without meaningful importance. So, for k_1 streamline projection method and potential flow solutions yield the real value.

The coefficient k_2 does not show the same comportment than k_3, although the probe is symmetric respect the X-axis parallel at the flow direction. The measures draw a decreasing curve, but with a slope smaller than what k_3 shows. At $Re = 13000$ the curve makes a strange jump of 0.5 units leaving far away the previous trend, finishing the sequence at -0.32. Almost 0.1 units of difference of the expected value, in comparison with k_3.

Huge differences are observed among the outer hole coefficients k_2 and k_3. The coefficient k_3 presents a curve with a very clear and progressive decreasing slope with a degree of dispersion almost negligible, between the values -0.1 and -0.4. From $Re = 12000$ the curve becomes a horizontal line that approach at -0.41.
The big diameter of the lateral holes could explain these differences respect the numbers calculated with streamline projection method or with potential flow, because the holes can be sensig a share of the total pressure.

Direction coefficient displays a significant deviation respect the expected value $k_\beta = 0$. This fact is due to the error introduced by the hole coefficient k_2, that as has been mentioned above, presents a huge difference respect the comportment shown by the other hole coefficient k_3.

Total pressure coefficient presents a very plane comportment like k_1 does. With independence of the Reynolds number, all points are very close to zero, which is in agreement with the streamline projection method as well as with potential flow solution.

Static pressure coefficient shows how the fact to use the average of the outer holes helps significantly to reduce the scatter. Unlike of k_β that is calculated as the rest of k_2 and k_3, k_s uses the mean. Thus if the trend of the static pressure coefficient is clear, is thanks basically at the good behavior presented by k_3. Streamline projection method says that the value that would approach the curve must be 0.704, and from potential flow must -0.574. The gap between them is very important and any of them is close at the real value, $k_s = -0.25$. So streamline projection and neither potential

flow are useful to predict the behavior of static pressure coefficient.

The curve drawn by dynamic pressure coefficient is basically the same as the encountered for k_2 due to the way how it is calculated. Even the same jump of the points at $Re = 13000$ is observed. The main difference respect k_2 is that the Y-scale has moved up 1 positive unit, being now the range of the curve between 0.75 and 0.87. Neither the streamline projection method nor the potential flow solution correctly predict the behavior of k_d.

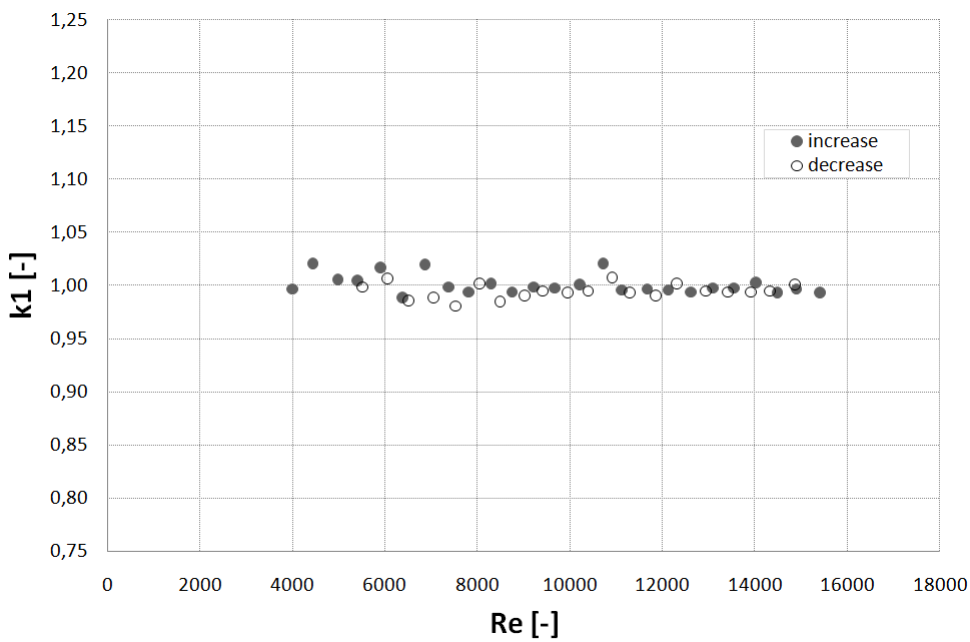

Figure 6.16: AVA 43 cylinder probe hole coefficient k_1

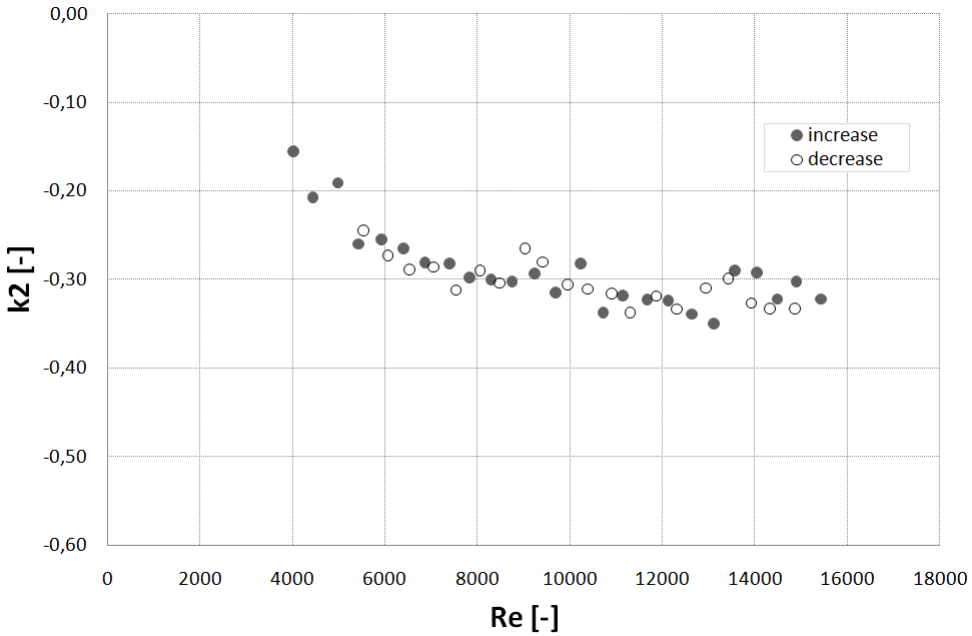

Figure 6.17: AVA 43 cylinder probe hole coefficient k_2

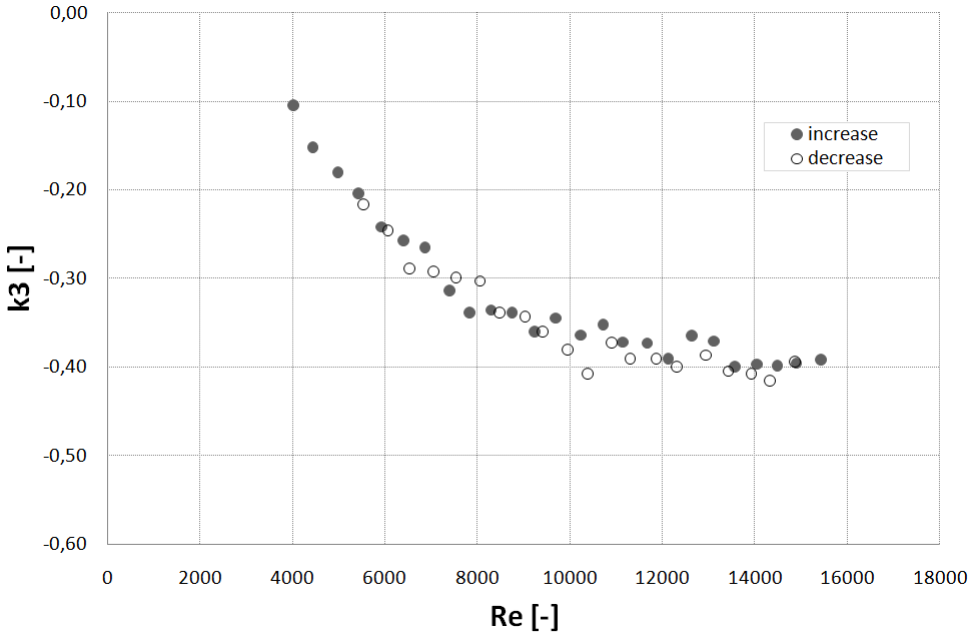

Figure 6.18: AVA 43 cylinder probe hole coefficient k_3

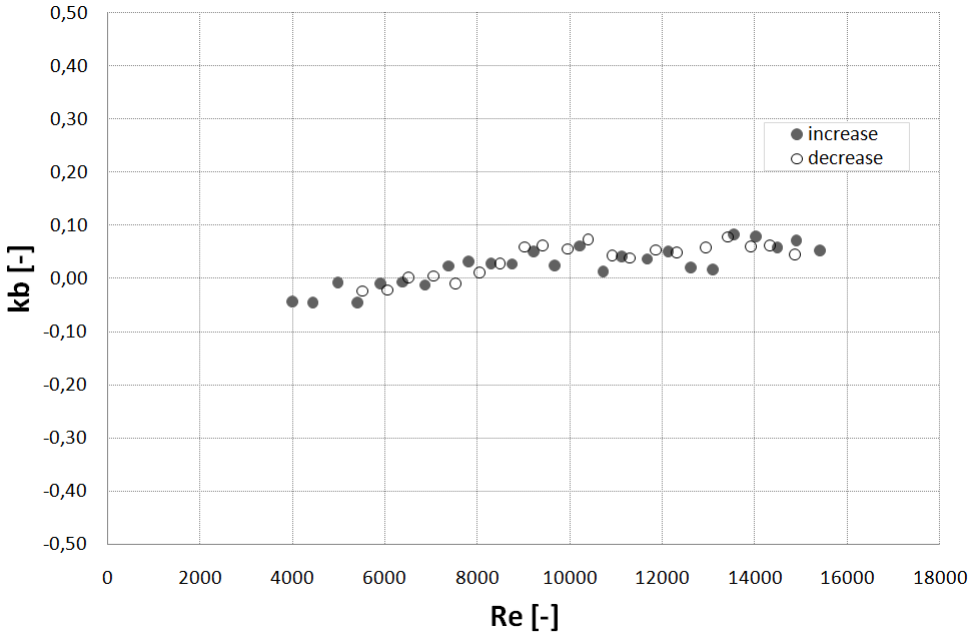

Figure 6.19: AVA 43 cylinder probe direction coefficient k_β

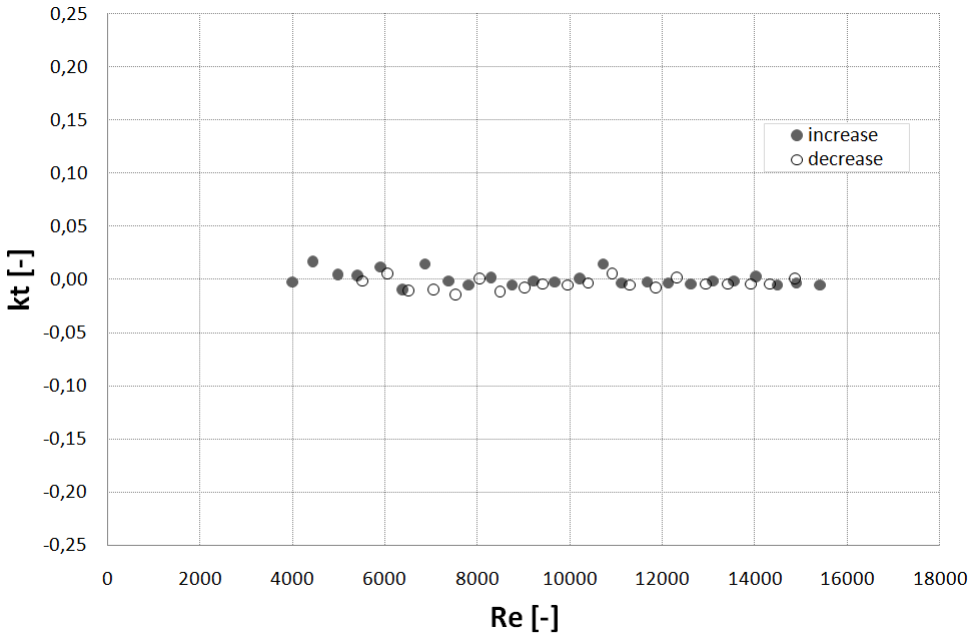

Figure 6.20: AVA 43 cylinder probe total pressure coefficient k_t

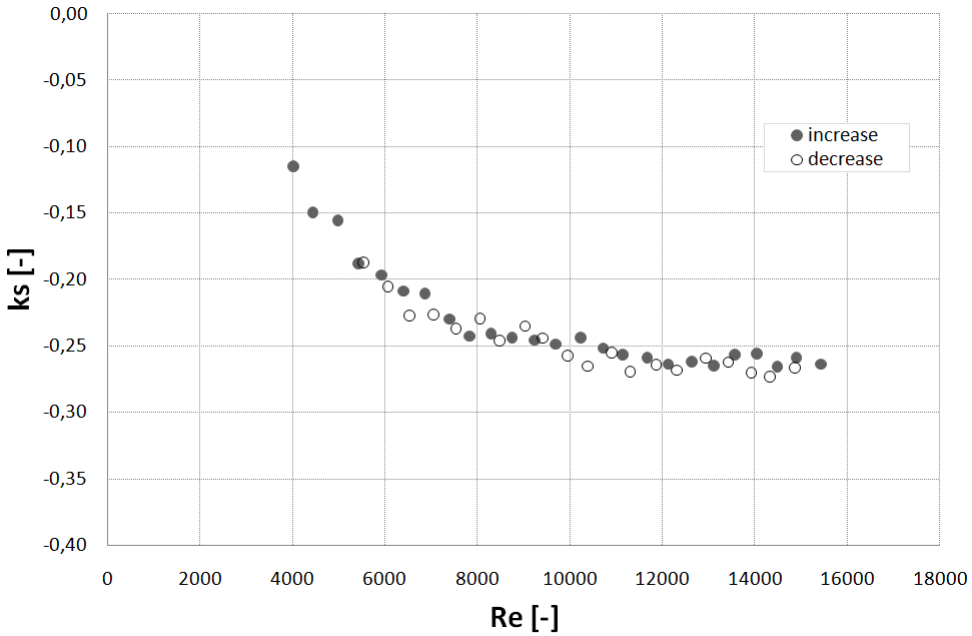

Figure 6.21: AVA 43 cylinder probe static pressure coefficient k_s

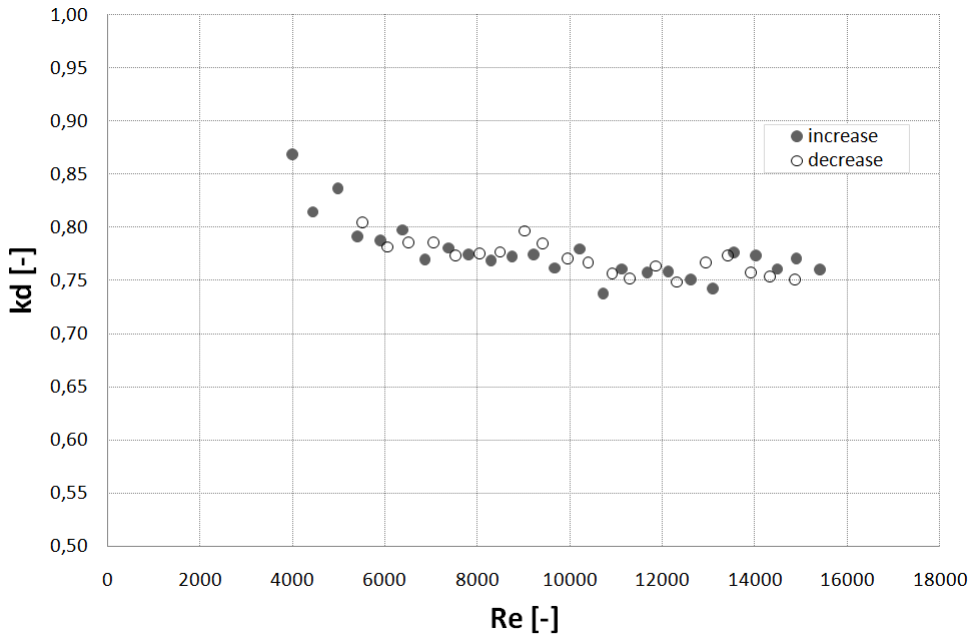

Figure 6.22: AVA 43 cylinder probe dynamic pressure coefficient k_d

Chapter 7

Conclusions

All the coefficients except k_1, k_t and k_β show variation respect Reynolds number. As it is mentioned at the previous chapter, under nulling conditions k_1 and k_t are equivalents because they measure the same magnitude, the stagnation pressure. They show a behavior completely plane with independence of the velocity of flow, either increasing or decreasing the velocity. The direction coefficient k_β is not so useful due to the experiment has carried out under nulling conditions, so its value must be always zero, over the entire Reynolds range.

For the rest of coefficients, in all of them are notes a peculiarity in common. At low airflow velocities they present, with greater or lesser degree and clarity, curves with a descendant inclination that stabilizes from a certain speed, from that point remains more or less constant until the end of range.

For a curve that draws the result of a division display an inclination, either posi-

tive or negative, means that the numerator not to vary in the same gives that makes the denominator. While that when a curve shows a plane behavior is because the variation of the numerator and denominator is constant.

The application practiced of this mathematical reasoning lies in the fact that all the coefficients used, defined by Treaster and Yocum, except the dynamic pressure coefficient, have the same denominator $k_1 - \bar{k}$, or $p_1 - \bar{p}$ if it is expressed as measured pressures. Which means that if the numerator does not vary with the same relation as the denominator does, even though the probe is under an homogeneous flow field, the vary of the pressures p_2 and p_3 are different as p_1. This phenomena is observed at Fig.7.1, which shows the relation of the numerator $\bar{p} - p$ respect the denominator $p_1 - \bar{p}$ of the measures read by SVUSS/3 cobra probe. The graph shows clearly that

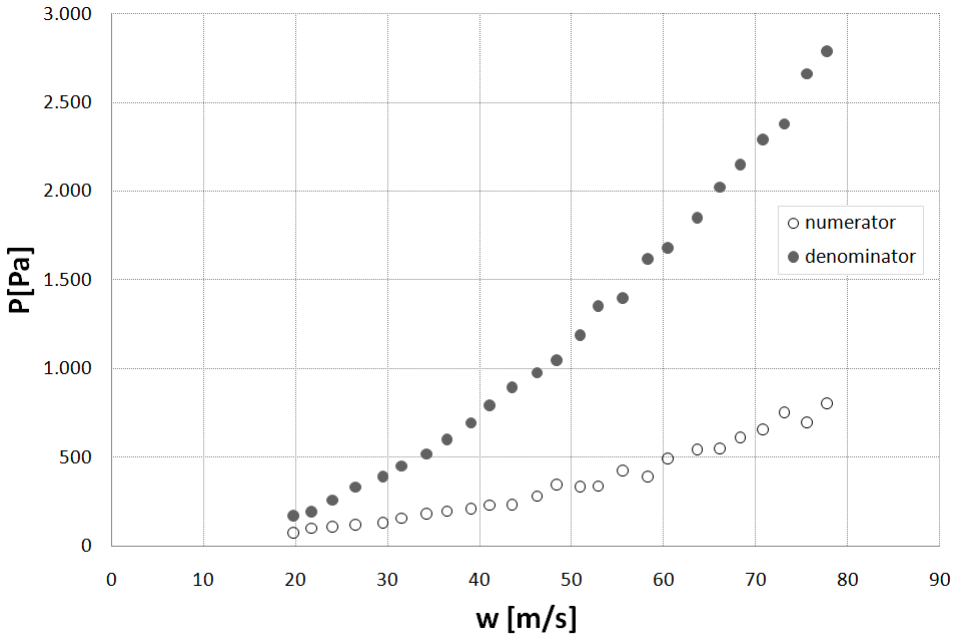

Figure 7.1: SVUSS/3 pressure evolution

$p_1 - \bar{p}$ presents a curve with a rising inclination, while the inclination of $\bar{p} - p$ remains more or less constant.

The results have shown quite good agree between the values calculated with streamline projection method and the values the curves approach when got stabilized as horizontal line. As it is a merely geometric method, the values that provides are constant. But if the process is inverted, from the measures it is possible to extract and calculate the geometric parameter as a function of them. Thus, it is possible to express how hypothetically vary the wedge angle versus the Reynolds number. Fig.7.2 show the vary of the wedge angle calculated using the mean of the two lateral hole coefficients k_2 and k_3, The overall conclusion that is extracted, is notes that from a

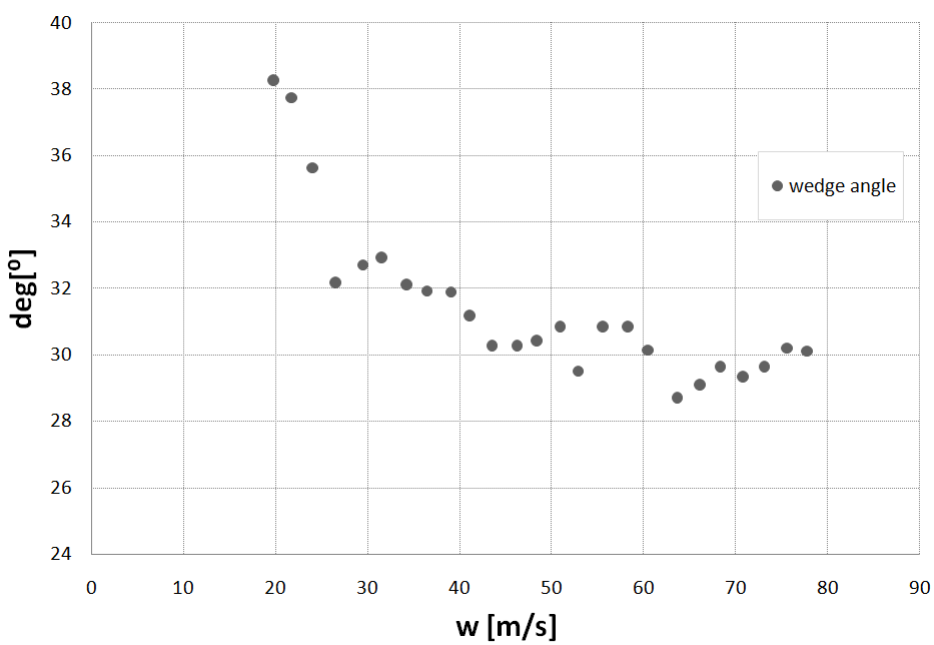

Figure 7.2: SVUSS/3 wedge angle evolution

certain speed, the wedge angle draws to its real value of $\delta = 30°$, and like the majority of coefficients shows a negative trend. The explanation of this phenomena is because at low Reynolds number a separation of the flow from the probe body is produced on the surface of the two side holes, which create an alteration of the pressure sensed by the outer holes. This phenomena was documented by Dominy and Hodson [1] as a factor that has a significant influence on the calibration.

The dynamic pressure coefficient k_d, which we suppose that it could display signs that permit us to confirm the suspicious that hysteresis can appear during the experiment, has not shown the expected results. The high degree of scatter makes that although there is some transition zones represented like a slight deviation of the values respect the natural trend, it is not evidence enough to affirm with certainty that it would be hysteresis. Due to the dispersion at these zones looks like a cloud of points. And there is no difference between those that were obtained increasing respect those that were obtained decreasing the Reynolds number.

It is possible that was committed the original sin, to wait a concrete results before carrying out the experiment. What has created some disappointment at not being matched with the award expected. In view of the results obtained, has happened the worst thing that could imagine, we cannot say with complete certainty nor deny that the hysteresis is a factor to be taken into account in the calibration of the probes used in this study. At the same time that it is not understood the big difference of the results respect the calibration data provided by the manufacturer of SVUSS/3.

I propose therefore a modification in the method of calculating k_d. Looking at the equation that defines it Eq.(7.1). It depends of the coefficients k_1 and k_2. My proposal is that instead of using only the coefficient k_2, it would be more advisable to use the average of both side coefficients k_2 and k_3. Because as it can be checked at the previous chapter, even though the values of k_2 and k_3 should be equals due to the symmetry of the probe, they are significantly. And the degree of scatter is also different. Thus the formula must be the following,

$$k_d = \frac{p_t - p}{p_1 - \bar{p}} = \frac{1}{k_1 - \bar{k}} \tag{7.1}$$

The aim of reduce the scatter and to have the absolute certainty that the measurements are going correctly, the experiment was reproduced two times. And for one probe even three times. Some modifications into the software of data acquisition were introduced, decreasing the sampling frequency in order to obtain measures during a longer time period. Thus is not necessary to take so many measures for each point, so with 30 single measures is enough.

As is it said previously, the motor-fan velocity was set manually in increments of 50rpm in a range from 400 up to 1600rpm. But in order to test the software changes, the experiment was repeated but this time setting the fan velocity in steps of 100rpm. Under these new conditions the experimental data obtained were very clear, with a low level of scatter.

Although is hard to imagine, with the yield results of the experiment, seems evident that the human action of set the velocity of the fan has a substantial influence in the scatter of the measures. There are no reasonable explanation of why there are such a big difference between to set the velocity in steps of 50rpm instead of 100rpm.

Some hypothesis are possible, maybe it is be due to inertial factors of the motor that actuate on the fan, or a supposed instability of the electronic system of DC that regulate the velocity of the motor, or a error induced by human action while set the velocity. At the last hypothesis, the effort of try to set the needle between two lines of the indicator may cause an alternative movement of acceleration and deceleration until find the concrete point. These facts make necessary a revision to try to improve the method and the experimental procedure of data acquisition. At following lines are explained some proposals of easy application which can provide important advantages:

Instead of to work only with the mean of the measures for each point, save all the data of the 30 measures done at each point. With them is possible to prepare a descriptive statistic treatment of the data to obtain, furthermore of the mean, very important parameters as standard deviation, maximum and minimum value measured. That would permit to plot them over Reynolds number and analyze their variations.

The most important parameter of all of them and which provide more information is the standard deviation. A high standard deviation indicates that the points are far of the mean, and a low deviation indicates that the points are close to the mean. Hence, it gives a degree of the stability of the flow field at the same time permit identify transition zones from laminar (low deviations) to turbulent regimes (high deviations). Also can be useful as an element to try to prove the hysteresis observed in this work. Thus, a low standard deviation at this zone would mean that the degree of scatter is low, thus the differences among increase and the progressive decrease of the velocity are due to hysteresis.

Bibliography

[1] **Dominy, R.G. and Hodson, H.P.** *An Investigation of Factors Influencing the Calibration of Five-Hole Probes for Three-Dimensional Flow Measurements. ASME Journal of Turbomachinery*, Vol.115:513–519, 1993.

[2] **Lee, S.W and Jun, B.J**. *Effects of Reynolds Number on the Non-Nulling Calibration of a Cone-Type Five-Hole Probe. Proceedings of 2003 ASME TURBO EXPO: Power for Land, Sea, Air, June 2003, Atlanta, USA.*

[3] **Lerena, D. and Willinger, R.** *Experimental Calibration of Three-Hole Pressure Probes with Different Head Geometries.*

[4] **Mittal,S. and Saxena,P.** *Prediction of Hysteresis Associated with the Static Stall of an Airfoil. AIAA Journal*, Vol.35:933–935, 2000.

[5] **Reneau,L.R., Johnston,J.P. and Kline,S.J.** *Performance and Design of Straight, Two-Dimensional Diffusers. Journal of Basic Engineering*, Transactions of the ASME:141–150, March 1967.

[6] **Schewe, G.** *Reynolds-number effects in flow around more-or-less bluff bodies. Journal of Wind Engineering and Industrial Aerodynamics*, Vol.89:1267–1289, 2001.

[7] **Sitaram, N., Lakshminarayana, B. and Ravindranath, A.** *Conventional Probes for the Relative Flow Measurement in a Turbomachinery Rotor Blade Passage. ASME Journal of Turbomachinery*, Vol.103:406–414, 1981.

[8] **Treaster,A.L. and Yocum,A.M**. *The Calibration and Application of Five-hole Probes. ISA Transacions*, Vol.18:23–34, 1979.

[9] **Willinger, R.** *A Three-hole Pressure Probe Exposed to Wall Proximity Effects: Experimental, Numerical and Analytical Investigation. Conference on Modelling Fluid Flow (CMFF'06), September 2006, Budapest, Hungary.*

[10] **Willinger, R. and Haselbacher, H.** *A Three-hole Pressure Probe Exposed to Velocity Gradient Effects - Experimental Calibration and Numerical Investigation. Conference on Modelling Fluid Flow (CMFF'03), September 2003, Budapest, Hungary.*